

# General air temperature and humidity features of local climate zones: A multi-city observational study in eastern China



Xiaoshan Yang<sup>a,b,c,\*</sup>, Shasha Xu<sup>b</sup>, Lilliana L.H. Peng<sup>b</sup>, Yuan Chen<sup>b</sup>, Lingye Yao<sup>c</sup>

<sup>a</sup> School of Geographical Sciences, Nanjing University of Information Science & Technology, Nanjing, China

<sup>b</sup> School of Architecture, Nanjing Tech University, Nanjing, China

<sup>c</sup> State Key Laboratory of Subtropical Building Science, South China University of Technology, Guangzhou, China

## ARTICLE INFO

### Keywords:

LCZ  
Air temperature  
Humidity  
Fixed station  
Multi-city study  
Heat wave

## ABSTRACT

The local climate zone (LCZ) scheme has been widely applied in urban climate studies. However, most field observations were conducted in individual cities and focused solely on air temperature. Few investigations have focused on the general climatic features of LCZs. This study aimed to obtain a reliable understanding of the air temperature and humidity features of LCZs by conducting multi-city observations. Towards this goal, fixed stations were established using temperature/humidity loggers deployed at 17 pairs of urban and rural sites in 15 cities of eastern China for one year. All the rural reference sites were LCZ D (low plants). Differences in air temperature ( $\Delta T$ ) and humidity ratio ( $\Delta W$ ) between the urban and rural sites (LCZ X – LCZ D) were analyzed on multiple time scales (diurnal, seasonal, and annual). In addition, we assessed urban-rural differences in the frequency and duration of heat and cold waves and the effects of local urban climates on building energy demands and human thermal stress. The results showed that: (1) the nocturnal  $\Delta T$  values for 'ideal' days (calm and clear days) exhibited distinguishable differences among different LCZ types, but approximately similar magnitudes for urban sites belonging to the same LCZ type; (2) the analysis of  $\Delta W$  revealed that moisture deficits and excesses were common occurrences in urban sites across cities; and there was no discernible pattern in  $\Delta W$  among LCZs; (3) compared to their rural counterparts, all urban sites exhibited remarkable increases in heat-wave incidence, cooling energy demand, and heat exposure risk. These findings will help better understand the general climatic features of LCZs and develop adaption strategies.

## 1. Introduction

Climates in urban areas are distinguished from those of their rural surroundings by differences in surface temperature, air temperature and humidity, air flow, air quality, precipitation, etc. (Oke et al., 2017). In recent decades, urban climates have received increasing attention because they have been shown to significantly impact urban ecology (Grimm et al., 2008; Oke et al., 2017; Kabano et al., 2021; Zhao et al., 2022a), economy (Estrada et al., 2017; Liu et al., 2020), energy consumption (Li et al., 2019; Yang et al., 2020c), and public health (Laaidi et al., 2012; Ho et al., 2023). Improving our understanding of urban climates is essential for developing adaption and mitigation strategies to counter their negative impacts.

The best-documented urban climatic phenomenon is the urban heat island (UHI) effect, which is defined as the urban-rural

\* Corresponding author at: School of Geographical Sciences, Nanjing University of Information Science & Technology, Nanjing 210044, China.  
E-mail address: [yangx@nuiist.edu.cn](mailto:yangx@nuiist.edu.cn) (X. Yang).

temperature differences at the surface, in the air, and in the substrate (Oke et al., 2017). Traditionally, the UHI is described using screen-height (1–2 m above ground) air temperature differences between urban and rural areas. However, as objects of scientific analysis, the terms ‘urban’ and ‘rural’ are vague and the simple urban-rural divisions are inadequate when characterizing intra-urban and intra-rural temperature differences (Stewart, 2011; Stewart and Oke, 2012). To address this inadequacy, the local climate zones (LCZ) system was proposed to provide a climate-based, objective classification system of urban and rural sites for temperature studies (Stewart and Oke, 2012). LCZs are defined as regions of uniform surface cover, structure, material, and human activity that span hundreds of meters to several kilometers. The LCZ system classifies urban and rural landscapes into a standard set of 17 LCZ classes, namely ten built types (LCZs 1–10) and seven land cover types (LCZs A–G). Each LCZ class has a characteristic screen-height temperature regime that persists year-round and is most often pronounced on calm, clear nights. The LCZ system aims to improve the basis of inter-site or inter-city comparisons of UHI magnitudes, and thereby facilitate the exploration of UHI causes and controls (Stewart and Oke, 2012).

In recent years, a number of investigations on the features of near-surface air temperature ( $T$ ) contrasts among LCZs have been implemented in cities worldwide, including Madrid, Spain (Núñez-Peiró et al., 2021); Dijon, France (Richard et al., 2018; Emery et al., 2021); Londrina, Brazil (Anjos et al., 2020); Nagpur, India (Kotharkar and Bagade, 2018); Nanjing, China (Yang et al., 2018); and Hong Kong, China (Shi et al., 2018). In these studies, in-situ  $T$  measurements at fixed stations or by mobile traverses, or a combination of the two, have most commonly been used. Some general features can be drawn from these previous studies. At nights of the days that are ideal for UHI formation (e.g., calm winds and clear skies), most LCZ classes are found to present distinguishable temperature regimes that are associated with their surface structures and covers. Nocturnal  $T$  differences between LCZ classes with significant differences in site properties are typically much greater than those between LCZ classes with less physical difference (Leconte et al., 2015; Fenner et al., 2017). For example, the nocturnal  $T$  in zones with compact buildings (LCZs 1–3) are significantly higher than those of open urban zones (e.g., LCZs 4–6) or natural zones (e.g., LCZs A, B, D) (Lehnert et al., 2015; Skarbit et al., 2017; Yang et al., 2018; Beck et al., 2018). Despite the general trends identified in previous studies, the specific values of  $T$  differences between the same pairs of LCZ classes can be quite variable among studies (Skarbit et al., 2017; Yang et al., 2018). Apart from studying  $T$  differences between different LCZ classes (inter-LCZ differences), the  $T$  differences between sites that belong to the same LCZ class (intra-LCZ differences) have also been investigated. Most of the intra-LCZ difference investigations were conducted in European cities, including in Olomouc, Czech Republic (Lehnert et al., 2015); Szeged, Hungary (Skarbit et al., 2017); Berlin, Germany (Fenner et al., 2017); and Nancy, France (Leconte et al., 2015). These studies revealed considerable intra-LCZ variability, which was especially pronounced at night. One possible cause for such variability could be microscale heterogeneity, such as building density and surface cover (Stewart et al., 2014; Fenner et al., 2017). To address such variability, it is recommended to use spatially averaged  $T$ , or temperatures from sites that are well representative of the local surroundings (Stewart et al., 2014). Overall, previous studies have shown that the LCZ system can be used as an effective classification framework for local temperature studies, but inter-study and inter-site variability requires more investigations.

Although significant progress has been made in understanding the thermal behaviors of LCZs, more attention should be paid to the following aspects. First, most previous investigations of  $T$  differences among LCZs were single-city studies, so it is necessary to conduct multi-city investigations to obtain a reliable understanding of general climatic features of LCZs. Furthermore, although the LCZ system improves the consistency and accuracy in urban climate reporting, it is still difficult to directly compare the quantified results from different studies. This is because there are large discrepancies among studies in LCZ class determination, observational schemes and methods, synoptic condition selection, study periods, and data processing. Conducting multi-city investigations following a consistent scheme will effectively reduce such discrepancies, and thus is expected to provide more reliable understanding of LCZs. Despite the need, there are very few multi-city investigations of  $T$  differences among LCZs. The main reasons are the difficulties and costs of setting up and maintaining observation networks across cities. The study by Chen et al. (2021) utilized the data from the National Meteorological Stations (NMSs) network to investigate thermal behaviors of various LCZs throughout China. The NMSs situated within typical LCZs were selected for their analysis, allowing them to take advantage of the availability and accessibility of the data provided by the China Meteorological Data Service Center (*China Meteorological Data Service Centre (CMDC)*, 2022). However, the representativeness of these NMSs for their LCZs, especially built-type LCZs, is doubtful. Typically, NMSs were established for monitoring synoptic conditions of a geographic region, which means the instruments surroundings are generally standardized (e.g., flat open ground covered with short grass, well away from obstacles like buildings and trees). Even if the NMSs are embedded in built-type LCZs, the microscale surroundings of the instruments are different from the built-up areas where they are located. The study by Jiang et al. (2022) used data collected from the urban automatic weather stations (AWSs) networks of nine cities in China to investigate LCZ  $T$  differences. However, the data of urban AWS networks generally are not freely available. In addition, many urban AWSs have been placed over short grass in open spaces such as parks and playing fields (Oke, 2006). As a result, these stations might also be insufficiently representative of compact built-type LCZs. The guiding principle proposed by Oke (2006) suggested that a station for urban local climate observation should be sited in the place where the environment within a microscale radius is approximately representative of the local-scale environment of the locality. In summary, using the data from existing stations that were originally not designed for LCZ observation introduces the issue of insufficient representativeness. Second, most previous studies of LCZ differences focused on air temperature, while few studies investigated LCZ differences in other climatic elements such as humidity and wind. The circumstance might be related to the fact that the LCZ scheme was originally developed for studying near-surface air temperature. Based on long-term observations from fixed stations, two studies investigated the spatio-temporal patterns of air humidity of LCZs in the cities of Novi Sad, Serbia (Dunjić et al., 2021) and Nanjing, China (Yang et al., 2020b). These studies reported that there were discernible patterns in air humidity differences among LCZs which were correlated with  $T$  differences, synoptic conditions, and site properties. Although the two cities were significant different in background climate and size, generally consistent patterns in air humidity

differences between urban and non-urban LCZs were observed. Therefore, apart from temperature, the applicability of the LCZ concept to other climatic elements must be explored further. Third, previous studies mainly focused on the characteristics of LCZ  $T$  differences, and few investigated the possible influences of local-scale climates on, for example, building energy demands (Yang et al., 2020c) and human thermal stress (Unger et al., 2018b; Verdonck et al., 2018; Top et al., 2020; Giannaros et al., 2023). Despite their rarity, these studies demonstrated the usefulness of the LCZ system as an assessment tool for urban environments. To further extend the applications of the LCZ system, it is necessary to conduct multi-dimensional assessments of the possible influences of LCZs.

To address these aspects, this study investigated the air temperature and humidity features of LCZs across cities and their multi-dimensional influences. The one-year data sets used in this study are mainly comprised of two parts: 1) hourly  $T$  and relative humidity ( $RH$ ) data of the selected LCZ sites in 15 cities of eastern China collected from fixed stations set up by the authors, and 2) hourly background meteorological data of the 15 cities that were acquired from nearby NMSs. Based on these data, we sought to answer the following specific questions that have not been well addressed in previous studies:

- What are the general features of air temperature and humidity for LCZs across cities?
- Do sites in different cities with similar surface structure and cover (i.e., classified as the same LCZ class) exhibit approximately similar air temperature and humidity regimes?
- What are the differences among LCZs in terms of frequency and duration of temperature extremes (i.e., heat and cold waves)?
- What are the influences of local urban climates on building energy demands and human thermal stress?

We anticipate that this multi-city, long-term, observational study will improve our understanding of local-scale urban climates and help future city planning and management.

## 2. Data and methods

### 2.1. Study area

An overview of the study area is shown in Fig. 1. The study area, Jiangsu, is a coastal province located in eastern China (red area in

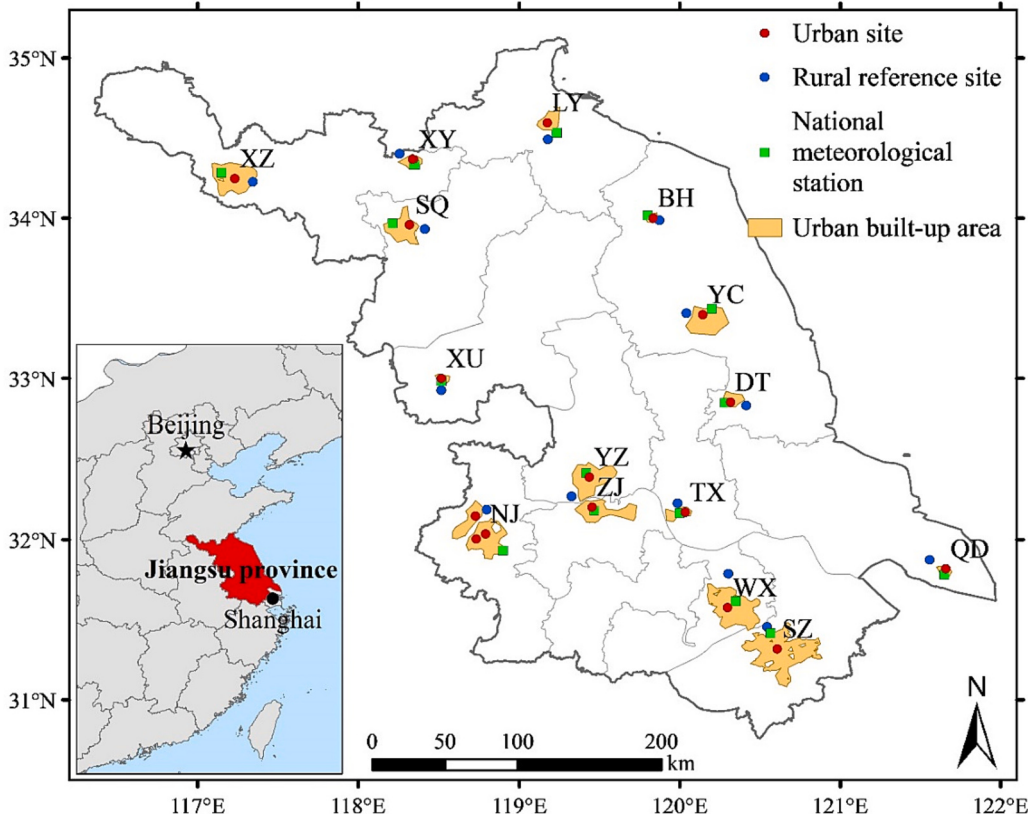


**Fig. 1.** Overview of the study area (Jiangsu province). The urban and rural sites selected for  $T$  and  $RH$  observation and the national meteorological stations used in this study. The two-letter abbreviations represent the names of the 15 cities (Table 1). Note that only the urban built-up areas where the urban sites are located are shown here.

**Fig. 1**). Jiangsu is part of the Yangtze River Delta Region, with a coastline of about 1000 km along the Yellow Sea. It borders the city of Shanghai to the south. According to the statistics provided by the provincial government, Jiangsu covers an area of 107,200 km<sup>2</sup>, and had a population of 85 million at the end of 2021. The province features a flat landscape, with plains accounting for 86.9%, and 93.9% of the total land area lying flat with slopes of 0 to 2 degrees. Most of the province is <50 m above sea level, and the elevation of the highest peak in the province is 624 m. Jiangsu is situated in a transition belt from a subtropical to temperate zone, with a humid subtropical climate to the south and a humid warm-temperate climate to the north. According to the Jiangsu Meteorological Bureau, the province features four distinct seasons, with temperatures averaging 0.5 to 3.9 °C in January and 26.7 to 28.6 °C in July. The annual average rainfall ranges between 800 and 1200 mm and is concentrated mostly in summer.

To examine the climatic features of LCZs across a variety of cities, we selected 15 cities in Jiangsu for investigation. These cities included the provincial capital city of Nanjing, eight prefecture-level cities, and six county-level cities. In China's administrative structure, county-level cities rank just below prefecture cities. These cities are generally smaller in terms of population, area, and economic activity compared to the prefecture-level cities in the same region. As shown in **Fig. 1**, the cities are widely distributed across the province. **Table 1** lists the relevant information of the cities. According to the data from the statistical yearbook for 2020 released by the Ministry of Housing and Urban-Rural Development of China, the urban built-up areas of the 15 cities ranged from 35 to 868 km<sup>2</sup>, with urban populations ranging from 0.27 to 6.82 million. There were no city-scale central heating systems in Jiangsu.

For each city, a pair of urban and rural sites were selected for local *T* and *RH* monitoring, except for the provincial capital city of Nanjing where three urban sites and one rural reference site were selected. Note that the same rural reference site was employed for two cities located near each other, Yangzhou (YZ) and Zhenjiang (ZJ) (see **Fig. 1**). In total, 17 urban sites and 14 rural reference sites were selected for the 15 cities. The nearest distance between the studied sites and the coastline was >20 km. We collected the hourly meteorological data from the NMS near each city, which are standard ground stations that are part of the World Meteorological Organization (WMO) network. **Fig. 1** shows the locations of the urban and rural sites and the NMSs. The urban extents of the 15 cities for 2020 were extracted from a global dataset of annual urban extents developed based on nighttime lights ([Zhao et al., 2022b](#)). Although weather stations located in suburban or rural areas have often been taken as the reference stations in the literature, we did not use the NMSs nearby the 15 cities as reference stations in this study. The reason was that, as shown in **Figs. 1, 14** of the 15 NMSs were situated within the urban built-up areas due to urban expansion in the past decades. As a result, these NMSs were subject to the influence of their urbanized surroundings and therefore were not suitable for use as reference stations for urban climate studies. Moreover, the heterogeneity in the local surroundings of the NMSs would undermine the goal of this study, which was to establish an inter-city comparison of urban climates. Therefore, for each city, a rural reference site was selected following the same criteria: 1) the rural site is located outside of the urban area and at least a few kilometers away; and 2) the area within a 1 km radius of the instrument at the rural site must be characterized as a featureless landscape of herbaceous plants/crops, with few buildings and paved surfaces, i.e., classified as LCZ D (low plants) according the LCZ system. Only the rainfall and wind speed data from the NMSs were used in this study. The urban sites in the 15 cities were chosen according to the LCZ definition ([Stewart and Oke, 2012](#)). Each urban site had generally uniform features within a 500 m radius from the instrument in terms of land cover, surface structure, material, and human activity. The following section provides detailed descriptions of the sites and field observations.

## 2.2. Study sites and observations

**Fig. 2** shows the satellite images of all 17 urban sites and three examples of rural reference sites. Not all images of the rural sites are presented here because they have similar, nearly indistinguishable features (LCZ D). Each image represents a 500 m radius area around the *T* and *RH* monitoring sensor. The major LCZ classes of the 17 urban sites spanned from LCZ 2 (compact mid-rise) to LCZ 5 (open mid-rise), which covered the common forms and landscapes of urban blocks in the cities of Jiangsu. **Table 2** summarizes the metadata

**Table 1**  
Relevant information for the 15 studied cities in Jiangsu province, China<sup>a</sup>.

City	Abbr.	City level	Urban built-up area (km <sup>2</sup> )	Urban population (million)
Nanjing	NJ	Provincial capital	868	6.82
Suzhou	SZ	Prefecture-level	481	4.26
Wuxi	WX	Prefecture-level	350	2.73
Xuzhou	XZ	Prefecture-level	290	2.08
Yancheng	YC	Prefecture-level	169	1.44
Yangzhou	YZ	Prefecture-level	186	1.24
Lianyungang	LY	Prefecture-level	223	1.12
Zhenjiang	ZJ	Prefecture-level	145	0.89
Suqian	SQ	Prefecture-level	104	0.88
Dongtai	DT	County-level	39	0.36
Binhai	BH	County-level	35	0.35
Xuyi	XU	County-level	45	0.32
Xinyi	XY	County-level	39	0.31
Taixing	TX	County-level	44	0.31
Qidong	QD	County-level	35	0.27

<sup>a</sup> The list of cities here is sorted by urban population size. The data of urban built-up area and urban population were extracted from the statistical yearbook for 2020 (in Chinese), released by the Ministry of Housing and Urban-Rural Development of China.



(caption on next page)

**Fig. 2.** Satellite images of all 17 urban sites and three examples of the rural reference sites. Each image shows a 500 m radius area around the *T* and *RH* sensor. The text to the top-left of each image is the designation of the site, where font colors are the same within each LCZ class (see the text at the bottom of each image, refer to Table 2 for further details).

of the 17 urban sites in the 15 cities. The LCZ class of each site was determined using both quantitative properties of the site and qualitative estimations. In this study, five quantitative properties were calculated for each site, namely building surface fraction (BSF), pervious surface fraction (PSF), impervious surface fraction (ISF), mean building height, and mean sky view factor (SVF) at the ground level. BSF and PSF were manually delineated and calculated based on high-resolution satellite images in the ArcGIS environment. ISF is defined as  $1 - (\text{BSF} + \text{PSF})$ . The exact heights of buildings in the cities were not available. Building heights were calculated based on shadow lengths of buildings in Google Earth images using the method developed by Qi and Wang (2014). Mean SVF values for the sites were computed using the DL-Light software (De Luminae, 2022) by modelling the site based on footprints and heights of buildings. Note that the LCZ system provides 10 indicators for LCZ classification. However, the remaining indicators, such as surface admittance and anthropogenic heat flux, were not estimated due to a lack of data. Qualitative estimations were conducted via visual inspection by comparing satellite and street-level images of the site with the sample photographs provided by the LCZ system (Stewart and Oke, 2012). Eventually, the 17 urban sites were classified into seven LCZ classes (Table 2), namely: LCZ 2<sub>4</sub>, LCZ 2<sub>3</sub>, LCZ 2<sub>E</sub>, LCZ 3, LCZ 4, LCZ 5, and LCZ 5<sub>E</sub> (where the subscript is the lower parent LCZ class).

One of the purposes of this study was to examine whether the sites in different cities with similar landscapes exhibit similar local climate regimes. Therefore, for a certain class of LCZ, we selected multiple sites from different cities, including LCZ 2<sub>3</sub> (two cities), LCZ 2<sub>E</sub> (six cities), LCZ 3 (two cities), and LCZ 5<sub>E</sub> (four cities). The LCZ sites selected from a single city (LCZ 2<sub>4</sub>, LCZ 4 and LCZ 5) were taken as transitional LCZ classes to observe how local climates vary with site properties. Hourly *T* and *RH* were collected from the fixed point at the center of each site (Fig. 2). At each point, a data logger (Onset HOBO U23-001 Pro v2) housed inside a matching radiation shield was mounted on a pole 2.3–2.5 m above the ground (Fig. 3). The data logger measured from −40 to 70 °C and from 0 to 100% *RH*, with

**Table 2**  
Metadata and descriptions of the 17 urban sites in the 15 cities<sup>a</sup>.

Site code <sup>b</sup>	Lat. Long.	Elev. (m)	BSF	PSF	ISF	H (m)	SVF	LCZ classification	Site features
WX	31.5763 120.2977	31	35%	11%	55%	40	0.39	LCZ 2 <sub>4</sub> : compact mid-rise with open high-rise	Mix of commercial towers and residential buildings
XY	34.3659 118.3415	41	44%	7%	49%	13	0.60	LCZ 2 <sub>3</sub> : compact mid-rise with compact low-rise	Mix of high-density housing (unplanned) and apartment blocks
XU	33.0001 118.5147	42	42%	15%	43%	11	0.55		
DT	32.8519 120.3164	19	35%	8%	56%	14	0.54	LCZ 2 <sub>E</sub> : compact mid-rise with paved ground	Inner city; mix of multistory residential and commercial buildings (apartments, offices buildings, hotels, retail shops)
ZJ	32.2027 119.4544	30	35%	11%	54%	15	0.42		
NJ <sup>1</sup>	32.0368 118.7912	13	34%	11%	55%	16	0.49		
YC	33.3971 120.1440	24	34%	4%	62%	14	0.51		
BH	34.0007 119.8337	14	32%	7%	61%	14	0.51		
LY	34.5941 119.1738	10	32%	8%	60%	16	0.50		
YZ	32.3906 119.4359	29	62%	4%	34%	8	0.30	LCZ 3: compact low-rise	Historic district; buildings are closely spaced (2–3 stories)
SZ	31.3187 120.6087	31	49%	14%	37%	9	0.40		
NJ <sup>2</sup>	32.0044 118.7329	8	14%	38%	48%	36	0.57	LCZ 4: open high-rise	Newly developed residential district; ample plant cover
NJ <sup>3</sup>	32.1478 118.7284	6	19%	36%	45%	23	0.55	LCZ 5: open mid-rise	
XZ	34.2464 117.2329	39	27%	13%	60%	18	0.51	LCZ 5 <sub>E</sub> : open mid-rise with paved ground	Residential district; row buildings (4–6 stories)
TX	32.1716 120.0330	33	26%	18%	56%	15	0.52		
QD	31.8181 121.6586	7	25%	12%	62%	16	0.49		
SQ	33.9589 118.3219	22	23%	23%	54%	19	0.52		

<sup>a</sup> Lat.–Latitude; Long.–Longitude; Elev.–Elevation; BSF–Building surface fraction; PSF–Pervious surface fraction; ISF–Impervious surface fraction; H–Mean building height weighted by building footprint area; SVF–Mean sky view factor at ground level.

<sup>b</sup> The list of urban sites here is sorted by site morphology (from compact to open, and then from high-rise to low-rise). Within the same LCZ type, sites are sorted by building surface fraction (from large to small). The three urban sites located in the same city, Nanjing, were designated as NJ<sup>1</sup>, NJ<sup>2</sup> and NJ<sup>3</sup>, respectively.

an accuracy of  $\pm 0.21$  °C and  $\pm 2.5\%$ . The position of each measuring point was carefully chosen with reference to the guide for meteorological observations in urban areas (Oke, 2006). All the measuring points had good exposure to their surroundings. Possible perturbation from nearby artificial heat sources, such as exhaust outlets of ventilating shafts or air conditioners, was avoided. Data are stored in the internal memory at 1-h intervals and downloaded twice every year. Field measurements started on September 1, 2020 and are continuing at present.

In comparison with previous studies, our observations had the following noteworthy characteristics: 1) In contrast to previous multi-city LCZ studies that used the data from existing weather stations (Chen et al., 2021; Jiang et al., 2022), the stations in this study were set up specially for monitoring local-scale  $T$  and  $RH$ , and therefore the observations were representative of the LCZs; 2) the relatively flat terrain of the entire study area (Jiangsu province) reduces topography-induced climate variability across cities; 3) the same selection criteria (Section 2.1) were applied for the selection of all rural reference sites, which ensured good homogeneity and comparability among reference sites; and 4) this study used the same type of data loggers at all sites, avoiding possible bias introduced by different types of instruments. In short, the high-quality field data improved the basis on which the inter-city comparison was made and thereby helped in obtaining a reliable understanding of the climatic features of LCZs.

### 2.3. Data sets

The following data sets are used in the study:

- (a) Hourly  $T$ ,  $RH$ , and humidity ratio ( $W$ ,  $g_{\text{water}}/\text{kg}_{\text{dry air}}$ ) for each site are used for the analysis of climate patterns of LCZs. A whole year of data from September 1, 2020 to August 31, 2021 were analyzed in this study.  $T$  and  $RH$  were directly measured at the sites. Site humidity ratio was calculated with the building energy simulation program EnergyPlus (The U.S. Department of Energy, 2022), using the measured  $T$  and  $RH$  from the site and the atmospheric pressure from the nearby NMS as the input data.
- (b) Hourly wind speed, rainfall, and atmospheric pressure for the same period were retrieved from the NMSs data of the 15 cities via the China Meteorological Data Service Center (China Meteorological Data Service Centre (CMDC), 2022). Note that the hourly NMS observations also included  $T$  and  $RH$  data, but these data were not used in this study, as explained in Section 2.1. The atmospheric pressure data were applied to calculate the site humidity ratio. The wind speed data were used to derive the Wind Chill temperature (see further explanation in Section 2.6.3). The rainfall data were adopted for identifying weather types. The weather data showed that, for five of the 15 cities, there were light snowfall events on one or two non-consecutive days during the study period. These days were treated as common rainfall days in the analysis.
- (c) The differences in the occurrences of heat and cold waves between urban and rural sites were also investigated. For this purpose, historical daily minimum and maximum  $T$  observations from the 15 NMSs for the period 1981–2010 were used to establish the thresholds for heat and cold waves (see further explanation in Section 2.6.1). The dataset was provided by the China Meteorological Data Service Center (China Meteorological Data Service Centre (CMDC), 2022).

### 2.4. Definition of urban-rural differences

In the analysis below, the differences in  $T$  and  $W$  between the 17 urban sites and their rural counterparts (LCZ X – LCZ D) are expressed as  $\Delta T$  and  $\Delta W$ , respectively. Here, LCZ X represents the LCZ classes of the urban sites (Table 2), while all rural reference sites are LCZ D (low plants). The  $T$ & $RH$  sensors' uncertainties ( $\pm 0.21$  °C/ $\pm 2.5\% RH$ ) may create minor errors that can impact the statistical detection of climatic events, such as UHI events. To address this issue, the magnitudes of  $\Delta T$  and  $\Delta W$  values were divided into two



**Fig. 3.** Installation of the temp/RH data logger with radiation shield, using the urban and rural monitoring points in Wuxi (WX) city for demonstration.

categories: insignificant and significant differences. Insignificant ranges for  $\Delta T$  and  $\Delta W$  are defined as:  $-0.5^{\circ}\text{C} \leq \Delta T \leq 0.5^{\circ}\text{C}$  and  $-0.3\text{ g/kg} \leq \Delta W \leq 0.3\text{ g/kg}$  (corresponding to a variation of 5% RH at  $10^{\circ}\text{C}$  at one standard atmosphere pressure). Then, significant differences were identified if the  $\Delta T$  and  $\Delta W$  values fell outside of these ranges (i.e., lower or higher values than the insignificant ranges). In this paper, we did not discuss RH differences between urban and rural sites because RH is strongly influenced by air temperature; as temperature increases, RH decreases. It has long been known in the literature that the RH is generally lower in the near-surface air in the built-up areas relative to their rural surroundings, particularly during the evening/night hours when strong UHI is present (e.g., [Unger et al., 2018a](#); [Yang et al., 2020b](#)). Instead, our focus was on exploring the variation in humidity ratio between urban and rural sites ( $\Delta W$ ).

## 2.5. Classification of weather conditions

Numerous studies have shown that synoptic conditions significantly influence urban-rural  $T$  differences. Hence, weather classification must be conducted from the perspective of urban climate. The study by [Yang et al. \(2020a\)](#) systematically evaluated the performances of four quantitative methods for identifying meteorological conditions that are favorable for UHI development based on three years of observations in Nanjing, China. Of the four methods, the diurnal temperature range ( $DTR$ ) in the rural area surrounding of a city was shown to be a good and easy-to-use indicator of daily maximum UHI intensity ( $UHII_{max}$ ), with larger  $DTR$  correlating with greater  $UHII_{max}$ . Their results showed that the threshold of  $DTR \geq 10^{\circ}\text{C}$  is appropriate for identifying the ‘ideal’ days for UHI development in Nanjing. Therefore, in this study, the  $DTR$  values at the rural sites were used to identify the ‘ideal’ days. Specifically, for the 15 cities, daily weather conditions during the study period were classified into three types: ‘ideal’ days, rainy days, and other days. ‘Ideal’ days are defined as the days with rural  $DTR \geq 10^{\circ}\text{C}$  and without rainfall. The days with rainfall (i.e.,  $> 0\text{ mm}$ ) are identified as rainy days. Other days are all the remaining days after excluding ‘ideal’ and rainy days. [Table 3](#) gives the number of the tree types of days for the 15 cities.

## 2.6. Indices for multi-dimensional assessments

Apart from the analysis of  $\Delta T$  and  $\Delta W$  features, three sets of indices related to the influences of local-scale climates on temperature extremes, building energy demands, and human thermal stress, were computed for all urban and rural sites. The comparison of urban-rural differences in these indices will help to understand the multi-dimensional influences of local-scale urban climates.

### 2.6.1. Heat waves and cold waves

Extreme-temperature anomalies, such as heat waves (HW) and cold waves (CW), affect human health and can lead to increases in mortality ([Laaidi et al., 2012](#); [Liu et al., 2022](#); [Ho et al., 2023](#)). To date, no universally accepted definitions for HW and CW exist. In this study, the methodology developed by [Lavaysse et al. \(2018\)](#) based on the persistence of events exceeding a percentile threshold was employed to detect HW and CW. The methodology defines HW (CW) as events of at least three consecutive ‘hot’ (‘cold’) days. In this context, a ‘hot’ day is a day whose maximum and minimum temperatures ( $T_{max}$  and  $T_{min}$ ) both exceed their threshold values. Similarly, a ‘cold’ day is a day whose  $T_{max}$  and  $T_{min}$  are both below their threshold values. HWs are detected during the warm half of the year (from April to September), while CWs are detected during the cold half of the year (from October to March). The methodology comprises two steps ([Lavaysse et al., 2018](#)): *Step 1* is the determination of the threshold values for heat and cold waves, which are calculated on daily intervals. The threshold values of daily  $T_{max}$  and  $T_{min}$  are computed from the observed  $T_{max}$  and  $T_{min}$  for that calendar day during a predefined climatological baseline period. In this study, historical daily  $T_{max}$  and  $T_{min}$  observations from the 15 NMSs for the 30-year period from 1981 to 2010 were used. For heat waves, the daily threshold values for  $T_{max}$  and  $T_{min}$  are defined as the 90th percentile of the 330 respective temperature values covering a span of 11 days centered on that day from the 30-year baseline period. For cold waves, the daily threshold values for  $T_{max}$  and  $T_{min}$  are defined as the 10th percentile of the 330 respective temperature values covering a span of 11 days centered on that day from the 30-year baseline period. *Step 2* is the calculation of the frequencies and durations of heat and cold waves. A heat or cold wave is identified when there are at least three consecutive days with both  $T_{max}$  and  $T_{min}$  above (for heat waves) or below (for cold waves) their daily threshold values (as described in *Step 1*). Note that two successive events separated by one day are pooled as a single event. The total duration (in days, not counting ‘pooled’ days) and frequency of heat or cold waves over the studied period was then computed.

The methodology utilizes the following key practices ([European Drought Observatory, 2021](#)). First, calendar day percentile-based threshold values derived from historical observations are used to determine ‘hot’ and ‘cold’ days. This means that the detected heat or cold waves are specific to the time of year and geographic location. Second, this methodology uses both  $T_{max}$  and  $T_{min}$ , rather than the more common practices which use only  $T_{max}$  or the daily mean temperature. This approach allows the strong impacts of nighttime

**Table 3**

Number of ‘ideal’, rainy, and other days for the one-year observational period for the 15 cities.

City	WX	XY	XU	DT	ZJ	NJ	YC	BH	LY	YZ	SZ	XZ	TX	QD	SQ
‘Ideal’ days	111	166	137	93	123	89	125	122	128	121	104	155	91	70	129
Rainy days	135	93	109	107	132	136	101	97	98	124	137	89	128	134	86
Other days <sup>a</sup>	119	106	119	165	110	140	139	146	139	120	124	121	146	161	150

<sup>a</sup> Other days are all the remaining days after excluding ‘ideal’ and rainy days.

temperatures on human health during heat waves to be taken into account, as recommended by the guidance from the WMO (McGregor et al., 2015). This methodology has been implemented in the European Drought Observatory for assessing heat and cold waves over Europe.

### 2.6.2. Cooling and heating degree hours

Degree hours, as well as degree days, are widely used for calculations relating to the effects of outside air temperature on building cooling and heating energy demands (Papakostas and Kyriakis, 2005). Degree hours include cooling degree hours (CDH) and heating degree hours (HDH), which measure by how much ( $^{\circ}\text{C}$ ) and for how long (in hours) outside air temperatures are higher/lower than specific baseline temperatures. CDH and HDH ( $^{\circ}\text{C}$  hours) are calculated with the formulas below:

$$\text{CDH} = \sum_{i=1}^n (T_{o,i} - 26)\alpha \quad (\alpha = 1 \text{ h, when } T_{o,i} > 26^{\circ}\text{C}, \text{ otherwise, } \alpha = 0)$$

$$\text{HDH} = \sum_{i=1}^n (18 - T_{o,i})\alpha \quad (\alpha = 1 \text{ h, when } T_{o,i} < 18^{\circ}\text{C}, \text{ otherwise, } \alpha = 0)$$

where,  $T_{o,i}$  is the temperature at the site on hour  $i$ ;  $n$  is the total number of hours studied; and 26 and  $18^{\circ}\text{C}$  are the cooling and heating baseline temperatures, respectively, according to the design standard for building energy efficiency in Jiangsu province (Jiangsu Phoenix Science Press, 2014).

### 2.6.3. Heat index and wind chill

In hot weather,  $RH$  is a major factor affecting human thermal sensation. The cooling effect of evaporative perspiration decreases when the ambient  $RH$  is high, which means the human body feels warmer in more humid conditions. The Heat Index (HI) temperature has been used to quantify what the temperature feels like to the human body by combining  $RH$  with  $T$ . The field of environmental health often uses HI to measure heat exposure risk (Table 4). In this study, the software developed by Anderson et al. (2013) was employed to calculate the HI of the urban and rural sites, using the site measurements of  $T$  and  $RH$  as inputs. There are various algorithms for HI calculation, and that used by the software has been validated by comparing with other algorithms (Anderson et al., 2013).

In cold weather, a strong wind can greatly increase the rate of heat loss from the human body, resulting in the perception of lower temperatures than the actual air temperatures. The Wind Chill (WC) temperatures estimate the temperatures felt by the body as a result of wind speed and actual air temperature. The WC temperature is often used to estimate frostbite risk when exposed to low temperatures (Table 4). Different formulas for WC calculation have been developed. Here, we used the formula developed by the U.S. National Weather Service (National Oceanic and Atmospheric Administration, 2022):

$$WC = 13.12 + 0.6215T - 11.37V^{0.16} + 0.3965TV^{0.16}$$

where,  $T$  is the air temperature in  $^{\circ}\text{C}$ ;  $V$  is the wind speed in km/h. The formula works for air temperatures below  $10^{\circ}\text{C}$  and wind speeds higher than 4.8 km/h. In this study, in-situ wind speeds at the sites were not measured. Therefore, the WC was calculated using the wind speeds from the NMS near each city and the site measured air temperatures as inputs. The HI and WC indices have been implemented in the U.S. National Weather Service to provide warning information. Table 4 lists the classifications of exposure risk for HI and WC indices, respectively, given by the U.S. National Weather Service (National Oceanic and Atmospheric Administration, 2022).

The assessment of outdoor heat stress using HI and WC temperatures has limitations. These indices do not consider factors such as solar radiation, long-wave radiation, and individual characteristics like metabolic activity and clothing (Coccato et al., 2016). However, in this study, we focused on the impact of urban-rural differences in temperature and humidity on human thermal stress, as we only measured these environmental variables. Therefore, we chose to use HI and WC indices instead of more comprehensive measures like the Physiological Equivalent Temperature (PET) (Hoppe, 1999) and the Universal Thermal Climate Index (UTCI) (Bröde et al., 2012).

**Table 4**  
Classification of exposure risk based on Heat Index (HI) and Wind Chill (WC) temperatures.

Heat Index			Wind Chill		
Classification	Range ( $^{\circ}\text{C}$ )	Effect on the body	Classification	Range ( $^{\circ}\text{C}$ )	Time to frostbite
Caution	$27 < \text{HI} \leq 32$	Fatigue possible	Low Risk	$-10 < \text{WC} \leq 0$	–
Extreme Caution	$32 < \text{HI} \leq 41$	Heat exhaustion possible	Moderate Risk	$-27 < \text{WC} \leq -10$	–
Danger	$41 < \text{HI} \leq 54$	Heatstroke possible	High Risk	$-39 < \text{WC} \leq -27$	10 to 30 min
Extreme Danger	$\text{HI} > 54$	Heatstroke highly likely	Very High to Extreme Risk <sup>a</sup>	$\text{WC} < -39$	<10 min

<sup>a</sup> More levels are defined in the original classification, but here we merged some levels as the WC in Jiangsu never went that low.

### 3. Results and discussion

#### 3.1. Hourly evolution

The features of hourly  $\Delta T$  and  $\Delta W$  were demonstrated using data from two cities: WX and SQ (Fig. 4). These cities were chosen as examples because they represent two patterns of  $\Delta W$ : urban moisture deficit (UMD) and urban moisture excess (UME). For the hourly changes of  $\Delta T$  and  $\Delta W$  in other cities, refer to Fig. S1 in the Supplementary Material.

The left column of Fig. 4 shows the results from WX (LCZ 2<sub>4</sub> – LCZ D), and the right column shows SQ (LCZ 5<sub>E</sub> – LCZ D). For the two cities, the diurnal cycles of  $\Delta T$  throughout the year exhibited similar patterns (Fig. 4a and b): from sunset to about 2 h after sunrise, the urban sites were significantly warmer than their rural counterparts, while relatively low and occasionally negative  $\Delta T$  values (urban cool islands, UCIs) were observed during daytime. The vertical stripes across the year indicated that magnitudes of  $\Delta T$  were regulated by synoptic conditions, with greater  $\Delta T$  values under favorable conditions for UHI development. Similar features in diurnal profiles of  $\Delta T$  have been observed in many studies (Skarbit et al., 2017; Yang et al., 2018; Anjos et al., 2020; Jiang et al., 2022; Shi and Zhang, 2022; Milošević et al., 2022; Núñez-Peiró et al., 2021; Beck et al., 2018).

In terms of  $\Delta W$ , two different patterns were found in the 15 cities, as represented by the results shown in Fig. 4c and d. For WX,  $W$  at the urban site was lower than at the rural site most of the time, with larger UMDs during daytime in the warm months (i.e., from May to October). In contrast, for SQ, there were frequent slight UMEs at the urban site, particularly during the period from June to August. The  $\Delta W$  results of all 17 urban sites showed that six urban sites exhibited patterns similar to that of SQ (UMEs occurring more frequently), while the rest displayed patterns similar to that of WX (UMDs occurring most of the time). The UMD pattern and dynamics revealed in this study agreed with previous single-city studies (Yang et al., 2020b; Dunjić et al., 2021). However, the UME pattern observed in six urban sites implied that UME is not an exception. Our results indicated that both UMD and UME are common patterns in urban sites across cities. It was also discernible that the  $\Delta W$  values showed diurnal and seasonal variability, which were further analyzed in Sections 3.4 and 3.5.

As shown in Fig. 4, there are discernible differences in  $\Delta T$  and  $\Delta W$  between the two daily time periods: from sunrise+2 h to sunset and from sunset to sunrise+2 h. Here, we defined the two time periods as ‘daytime’ and ‘nighttime’, respectively, consistent with previous studies (Yang et al., 2018; Yang et al., 2020b). These definitions of ‘daytime’ and ‘nighttime’ are applied in the analysis below.

The diurnal evolution of  $\Delta T$ , as shown in Fig. 4a and b, can be explained by the differences in warming/cooling rate between the urban and rural sites. The warming/cooling rate ( $^{\circ}\text{C h}^{-1}$ ) of a site at hour  $i$  is defined as the difference in temperature between hour  $i$  and the previous hour ( $i - 1$ ). Positive rates indicate warming, while negative rates indicate cooling. Fig. 5a shows the averages and standard deviations of the mean warming and cooling rates of the 17 urban sites and their rural counterparts for different weather conditions; Fig. 5b shows the corresponding averages and standard deviations of the mean  $\Delta T$ . Times have been respectively normalized to sunrise and sunset over the 1-year observation period. There were clear patterns in diurnal warming and cooling processes of the sites and diurnal evolutions of  $\Delta T$ . First, remarkable differences in warming and cooling rates of sites were observed

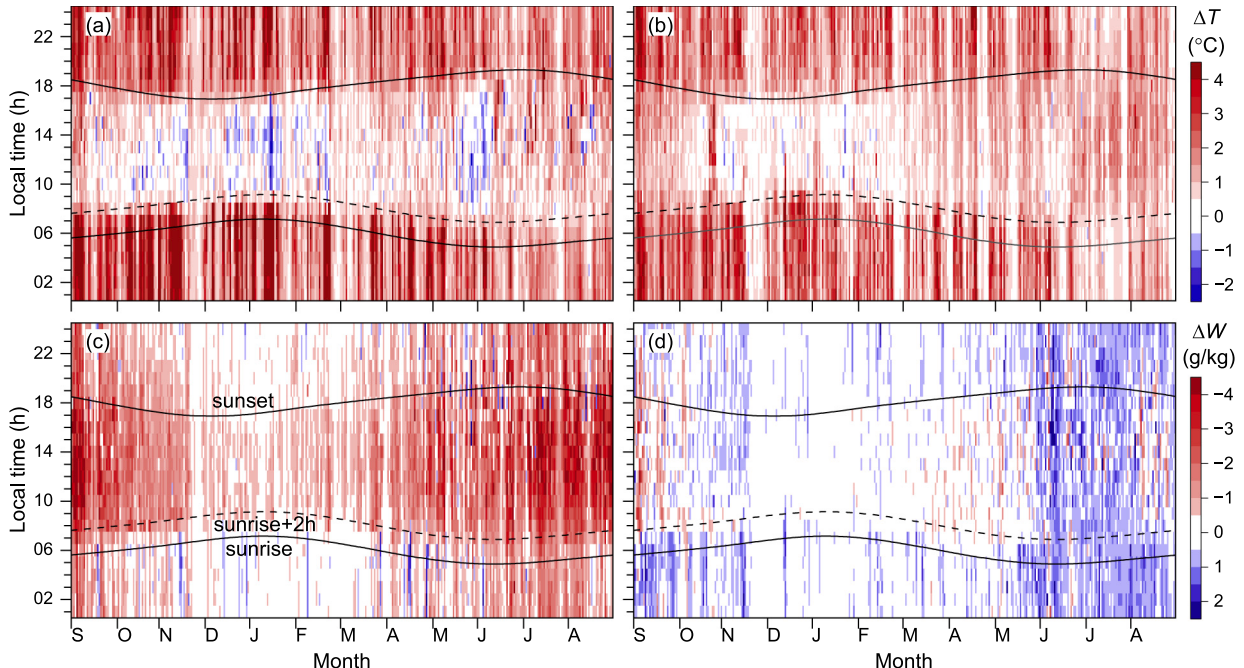


**Fig. 4.** Hourly evolution of  $\Delta T$  and  $\Delta W$  for the period from 1 September 2020 to 31 August 2021, using two cities as examples. The left column shows WX (LCZ 2<sub>4</sub> – LCZ D) and the right shows SQ (LCZ 5<sub>E</sub> – LCZ D).

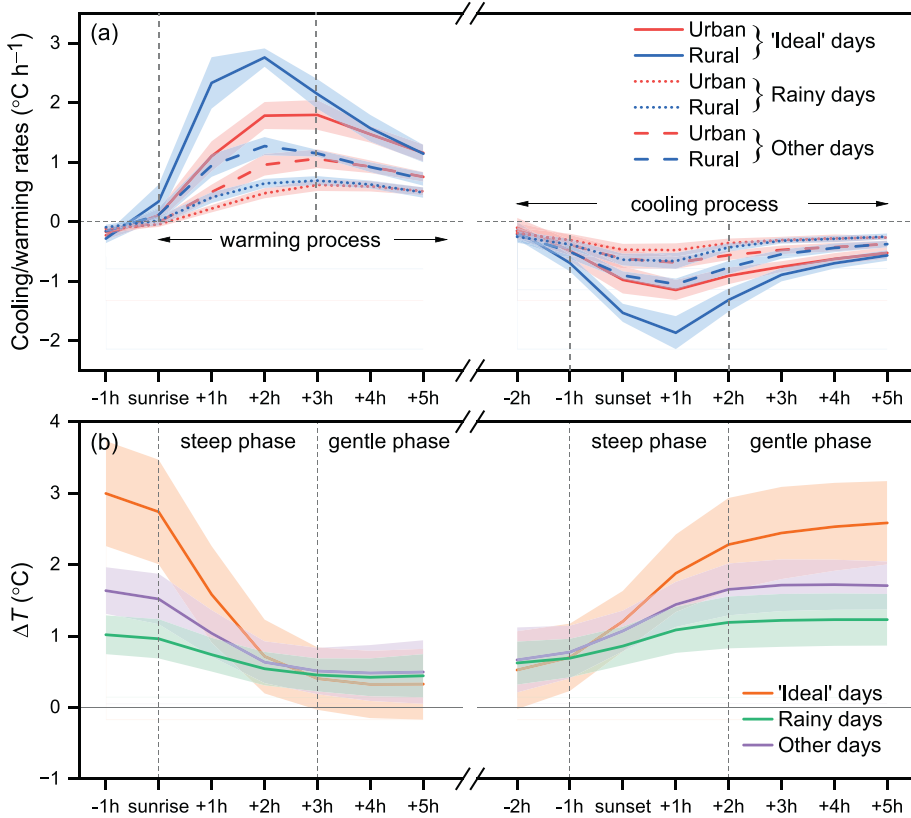


**Fig. 5.** Cooling and warming rates of the urban and rural sites in the 15 cities and the  $\Delta T$  results for the three weather types. Bold lines represent the averages, while the shaded areas indicate the corresponding standard deviations. Times are respectively normalized to sunrise and sunset over the 1-year observation period.

among the three weather conditions. For ‘ideal’ days, the warming/cooling rates of the sites and the urban-rural difference in warming/cooling rates were the greatest. Second, the warming process of the sites started at sunrise and ended at around two hours before sunset, and then the cooling process proceeded until sunrise. The curve of the warming rate generally exhibited an inverted ‘V’ shape, while the curve of the cooling rate showed a ‘V’ shape. Third, the significant urban-rural differences in warming rates generally occurred during the first three hours after sunrise, which corresponded to a period of steeply decreasing in  $\Delta T$  (erosion of UHI). The significant urban-rural differences in cooling rates were typically observed during the period from one hour before sunset to two hours after sunset, which corresponded to a period of steeply increasing in  $\Delta T$  (development of UHI). In contrast, relatively small and insignificant urban-rural differences in warming and cooling rates were observed during the rest of the day, corresponding to the two phases of gentle  $\Delta T$  changes (Fig. 5b). In short, compared to their rural counterparts, the much slower cooling (warming) rate at the urban sites during the evening (morning) hours caused the development (erosion) of UHIs. The two-phase (steep and gentle) nocturnal cooling and daytime heating revealed in this study generally agreed with previous studies (Milošević et al., 2022; Leconte et al., 2020).

### 3.2. Occurrence frequency

Fig. 6 shows the occurrence frequencies of different categories of  $\Delta T$  and  $\Delta W$  for daytime and nighttime (see Section 2.4 for descriptions of the categories). The occurrence frequencies of three categories of  $\Delta T$  were significantly different between nighttime and daytime (Fig. 6a). During nighttime, UHI events ( $\Delta T > 0.5 ^{\circ}\text{C}$ ) were the most frequent events for all 17 urban sites, ranging from 67% for site NJ<sup>3</sup> (LCZ 5) to 94% for site WX (LCZ 2<sub>4</sub>). Almost none of UCI events ( $\Delta T > -0.5 ^{\circ}\text{C}$ ) were observed during nighttime. During daytime, for all 17 urban sites, the frequencies of UHI events were lower and the times with insignificant differences ( $-0.5 ^{\circ}\text{C} \leq \Delta T \leq 0.5 ^{\circ}\text{C}$ ) accounted for 21–67%. Furthermore, for nine urban sites, UCI events were observed during 7–20% of the daytime. In short, UHI events occurred in most of the nighttime, while the frequencies of insignificant differences and UCI events accounted for considerable proportions of the daytime. This result was in line with previous findings in Nanjing (Yang et al., 2018).

Regarding the pattern of  $\Delta W$  (Fig. 6b), there were non-negligible occurrences of UME ( $\Delta W > 0.3 \text{ g/kg}$ ) for all 17 urban sites. Particularly, during the daytime, six urban sites (DT, ZJ, SZ, XZ, QD, and SQ) even showed significantly more frequent occurrences of UME than UMD ( $\Delta W < -0.3 \text{ g/kg}$ ). During daytime, the frequencies of UMD of all urban sites were higher while their UME frequencies were lower compared to those during nighttime. For all cities, there were insignificant urban-rural differences in  $W$  ( $-0.3 \text{ g/kg} \leq \Delta W$

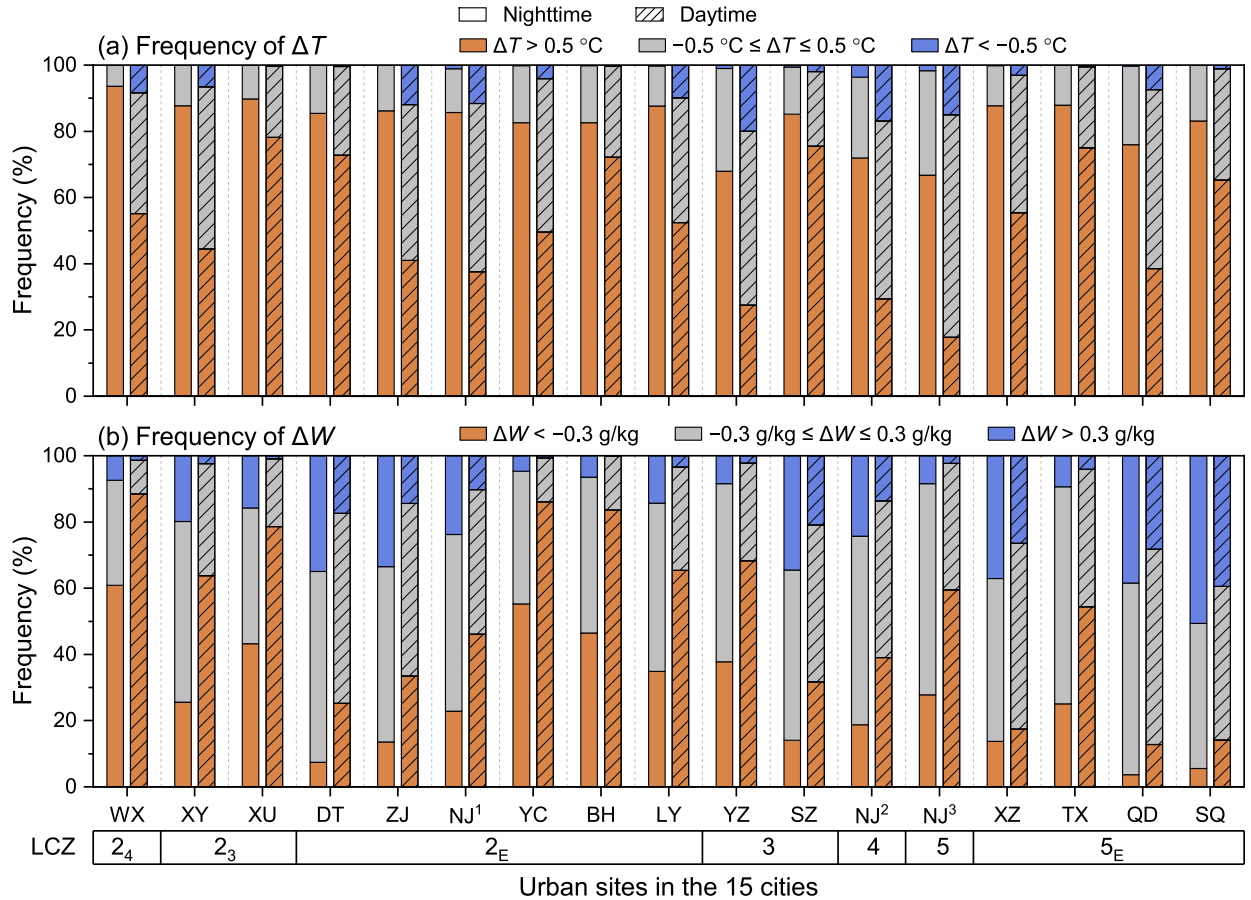


**Fig. 6.** Comparison of the occurrence frequencies of different categories of  $\Delta T$  and  $\Delta W$  between daytime and nighttime for the 1-year study period. Nighttime is defined as the period from sunset to sunrise+2 h (5035 h in total), while daytime is defined as the period from sunrise+2 h to sunset (3725 h in total).

$\leq 0.3 \text{ g/kg}$ ) accounting for considerable proportions of the total time. In addition, there were no clear patterns of inter- and intra-LCZ differences in the occurrence frequencies of the various  $\Delta T$  and  $\Delta W$  events.

### 3.3. Occurrence time

The analysis of the occurrence time of daily extremes of  $\Delta T$  and  $\Delta W$  is important for understanding local climates. Inspection of Fig. 6 revealed that, for most of the study period, urban sites featured positive  $\Delta T$  values, while both positive and negative  $\Delta W$  values were often observed at most urban sites. Therefore, we analyzed the occurrence times of daily extremes of maximum and minimum  $\Delta T$ , and negative minimum and positive maximum  $\Delta W$ . The daytime and nighttime periods were further divided into two halves, respectively. The first half of the daytime ends at 12:00, while the first half of the nighttime ends at 24:00. Fig. 7 shows the analysis of the occurrence periods of daily extremes over the study period. Clearly, for all urban sites, daily maximum  $\Delta T$  mainly occurred during nighttime, while daily minimum  $\Delta T$  mainly occurred during daytime (Fig. 7a). For the occurrence times of daily maximum  $\Delta T$ , there were no significant differences between the 1st and 2nd half of the nighttime period. A review of the UHI characteristics of many Asian and Australian cities showed that the maximum UHI intensities can occur before and after sunset or midnight or even during the daytime (Santamouris, 2015). Indeed, our results (Fig. 7a) showed that the maximum UHI intensities can occur at different times of the day. However, they clearly occurred mostly during nighttime. For daily extremes of  $\Delta W$ , the negative minimum values mostly occurred during daytime, while the positive maximum values mostly occurred during nighttime (Fig. 7b). Also, there were no significant differences between the 1st and 2nd halves of the nighttime or daytime. No clear patterns of inter- and intra-LCZ differences in the occurrence times of daily  $\Delta T$  and  $\Delta W$  extremes were found.

### 3.4. Annual mean differences

Fig. 8 shows the distributions of the nighttime and daytime mean  $\Delta T$  values. For all 17 urban sites, the nighttime mean  $\Delta T$  values showed significant differences among the three weather classifications, with the highest values occurring in ‘ideal’ days and the

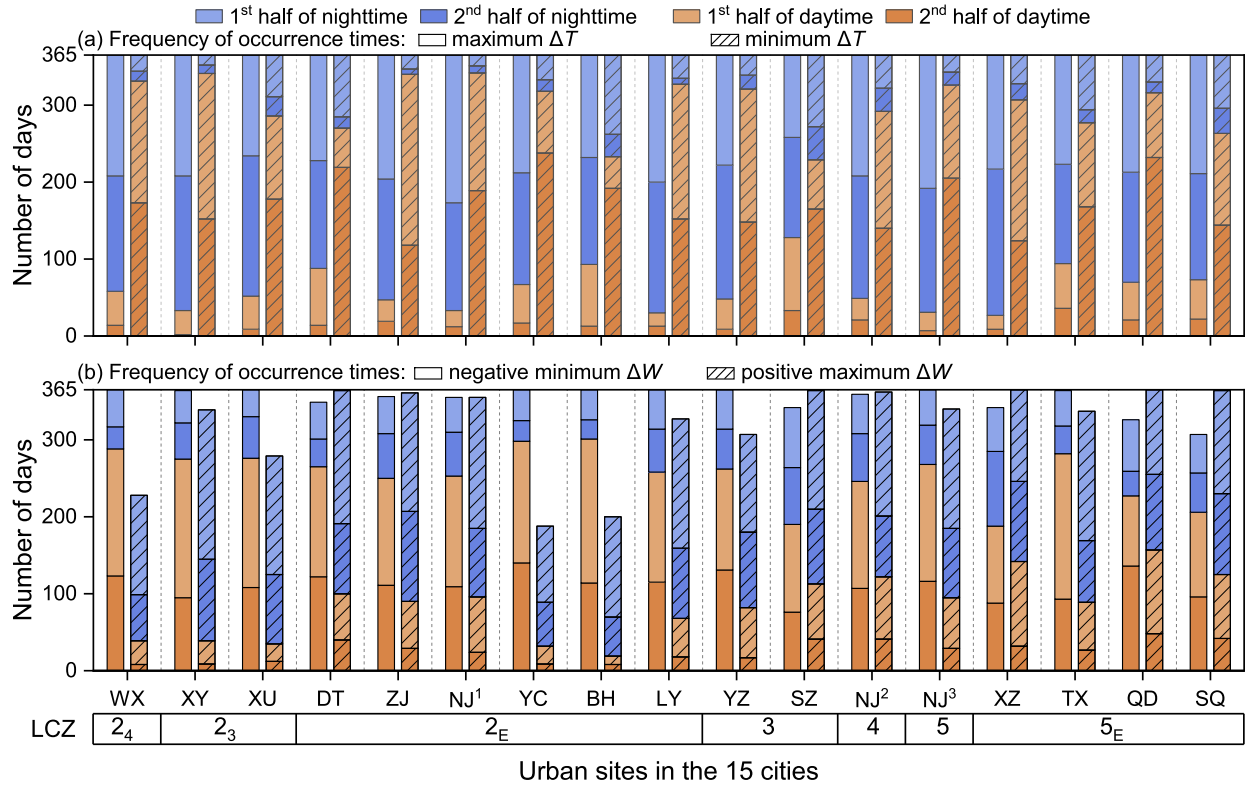


**Fig. 7.** Frequencies of occurrence times of daily extremes during the 1-year study period (365 days): (a) daily maximum and minimum  $\Delta T$ ; (b) daily negative minimum and positive maximum  $\Delta W$ . Note that there are some days without negative/positive  $\Delta W$  values, and therefore the cumulative number of days is <365 days in those cases.

smallest in rainy days. This proved that the *DTR*-based method was effective in classifying weather conditions for UHI analysis in different cities. The inter-site differences were also most significant during the nighttime periods of ‘ideal’ days, generally exhibiting distinguishable UHI intensities between different LCZ classes. The LCZs 2<sub>4</sub> (WX) and 2<sub>3</sub> (XY and XU) tended to have the highest UHI intensities, with mean levels around 3.5 °C. The LCZs 4 (NJ<sup>2</sup>) and 5 (NJ<sup>3</sup>) had the lowest UHI intensities, with mean levels around 1.5 °C. In general, for the nighttime periods of ‘ideal’ days, the urban sites of the same LCZ types presented approximately similar UHI intensities, even though these sites were situated in different cities with widely varying sizes and populations. These results indicated that the sites in different cities with similar surface structures and covers (i.e., classified as the same LCZ type) tended to exhibit similar approximate levels of nocturnal UHI intensities under ‘ideal’ weather conditions. In addition, we noted that the UHI intensities of LCZ 5<sub>E</sub> (XZ, TX, QD, and SQ) were greater than those of LCZ 5 (NJ<sup>3</sup>) for the nighttime periods of ‘ideal’ days. A comparison of satellite images of these sites (Fig. 2) and the site properties (Table 2) showed that the four LCZ 5<sub>E</sub> sites and the LCZ 5 site were similar in spatial structures (building/street morphologies), but discrepant in pervious surface fraction. This implied that both surface structure and surface cover (pervious or impervious) are important factors that lead to differences in local temperatures during nighttime.

In daytime, the inter-site differences in  $\Delta T$  values among the three weather classifications were much more moderate than those during nighttime. All urban sites featured weak daytime UHIs or UCIs. In short, the intensities of UHIs and inter-site temperature differences were most pronounced during the nighttime periods of ‘ideal’ days. During the nighttime of rainy days and the daytime under all weather conditions, the intensities of UHIs and inter-site temperature differences were moderate. We can further infer that city-scale heat maps of canopy UHI would exhibit the largest and most heterogeneous variability during the nighttime periods of ‘ideal’ days, while heat maps would appear more moderate and less heterogeneous during daytime under all weather conditions.

Fig. 9 shows the distributions of the nighttime and daytime mean  $\Delta W$  values. In comparison to the rural reference sites, both UME and UMD patterns were observed in urban sites. For instance, for both nighttime and daytime, seven sites (WX, XU, YC, BH, LY, YZ, and TX) featured UMD patterns, while three sites (XZ, QD, and SQ) were generally characterized as having UME patterns. These results further indicated that both UMD and UME were common patterns occurring at various urban sites of different cities. For all urban sites, the differences in  $\Delta W$  among three weather classes were generally insignificant during both nighttime and daytime. However, there were clear differences in  $\Delta W$  between nighttime and daytime. For all urban sites, the mean  $\Delta W$  in the daytime showed overall lower values than the nighttime (i.e., greater negative or smaller positive  $\Delta W$  values). In the daytime, with higher temperatures and solar radiation, much more water evaporated into the air at the rural sites than the urban sites due to their higher proportions of pervious surfaces. As a result, UMD values would be enlarged while UME values would be reduced. No clear patterns of inter-LCZ and intra-LCZ differences in  $\Delta W$  were apparent in either nighttime or daytime. For urban sites that belonged to the same LCZ type, such as LCZs 2<sub>E</sub>

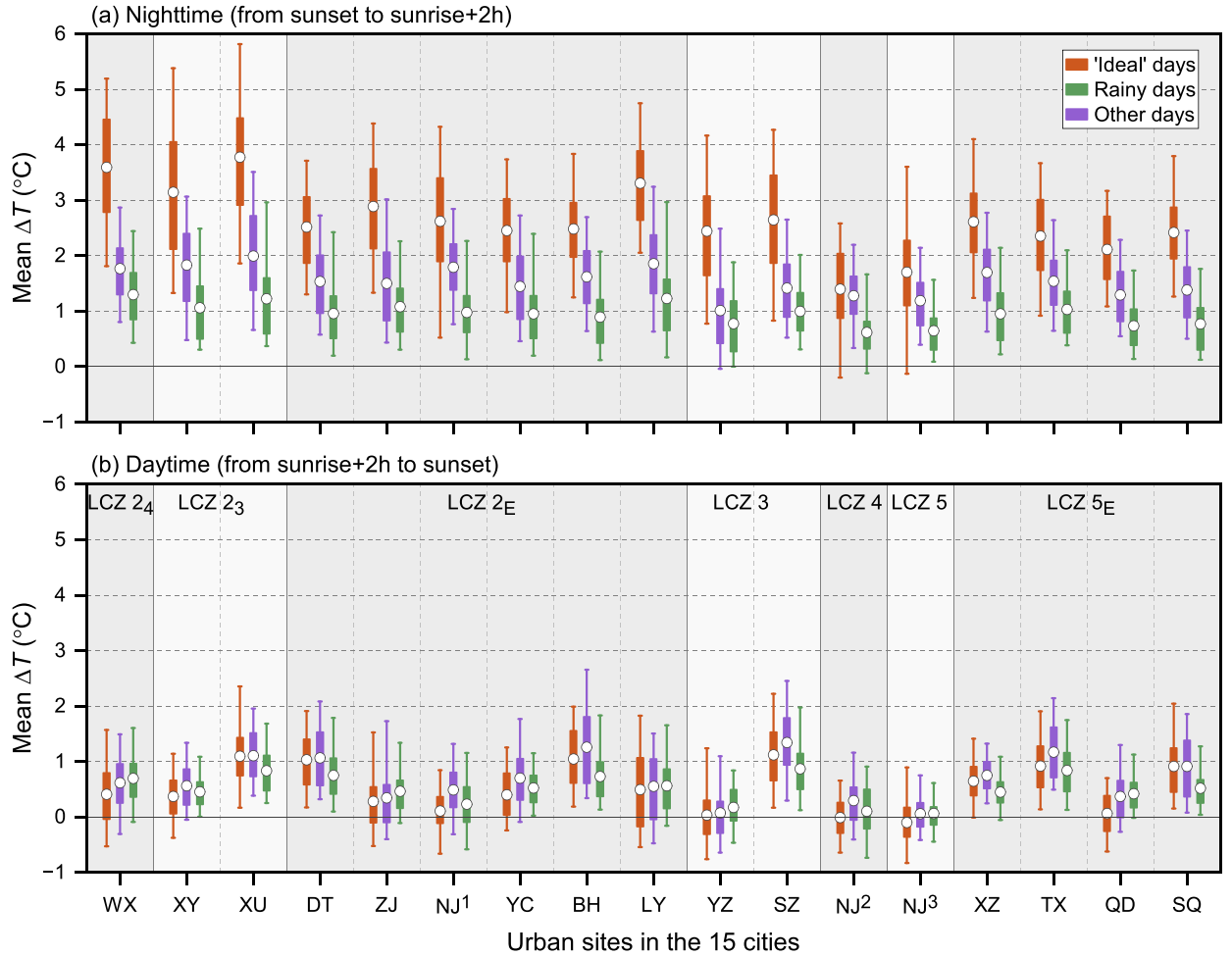


**Fig. 8.** Annual mean differences in  $\Delta T$  between the 17 urban sites and their rural counterparts (LCZ D) for the three types of days (see Table 3 for the number of each type of days). The urban sites classified as the same LCZ type are grouped by different background grey shades (see Table 2 for the descriptions of the LCZs). Each box encompasses the data between the 25th and 75th percentiles; the circles denote the means; and the whiskers represent the 5th and 95th percentiles of the data, respectively.

and 5<sub>E</sub>, certain sites manifested UMEs while others manifested UMDs. The causes of this variability remain unclear. Overall, the features and patterns of  $\Delta W$  were quite dissimilar to those of  $\Delta T$ . For example, no clear relationships were found between  $\Delta W$  and weather conditions nor between  $\Delta W$  and LCZ classes.

### 3.5. Seasonality

Fig. 10 shows the distributions of mean  $\Delta T$  and  $\Delta W$  for the 'ideal' days in the warm months (from April to September) and cold months (from October to March). During nighttime, differences in mean  $\Delta T$  between the warm and cold months were insignificant and lacked clear and consistent trends; while during daytime, the mean  $\Delta T$  values in the cold months were slightly smaller than those in the warm months (Fig. 10a). Our results showed that there was no significant or clear seasonality in nocturnal  $\Delta T$ , which differed from a previous review that reported higher UHI intensities commonly occur during the warm period of the year or during the dry season (Santamouris, 2015). In terms of the mean  $\Delta W$ , significant differences were observed between nighttime and daytime and between warm and cold months (Fig. 10b). For most sites, the urban-rural differences in  $W$  were larger during daytime and during warm months, as compared to nighttime and cold months, respectively. These patterns were consistent with the single-city observational studies (Yang et al., 2020b; Dunjić et al., 2021). The diurnal and seasonal variability in  $\Delta W$  was likely related to the fact that the pervious surface fractions of the urban sites were much lower than those of their rural counterparts. As a result, the urban-rural differences in the evaporation rate of water from surfaces will further intensify during daytime due to solar radiation and during warm months due to relatively high ambient temperatures.

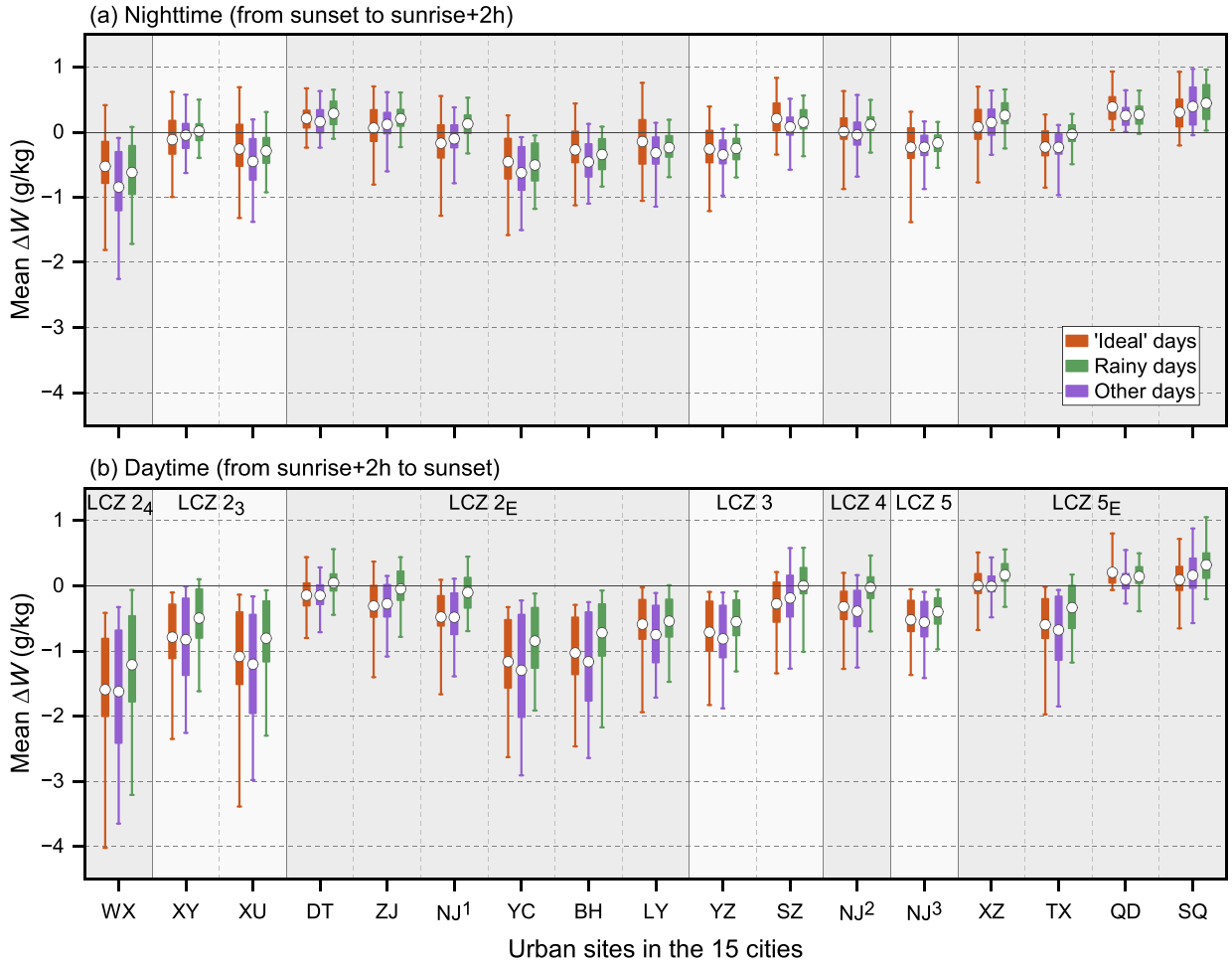


Fig. 9. The same as Fig. 8, but for annual mean differences in humidity ratio ( $\Delta W$ ).

### 3.6. Assessment indices

#### 3.6.1. HW and CW

According to the definitions of HW and CW provided in Section 2.6.1, the occurrence frequencies and cumulative days of HW and CW events at urban and rural sites throughout the 1-year period were determined (Fig. 11). For HW events, both the occurrence frequencies and cumulative days at urban sites were remarkably higher than those at the rural reference sites. At rural sites, only one HW event was recorded at three of the sites. In contrast, all 17 urban sites experienced one to five HW events with total durations ranging from 3 to 23 days. The results clearly indicated that urban sites experience more frequent and longer HW events relative to rural sites. Among the urban sites, there was significantly more variability in HW occurrence compared to their rural counterparts. For example, LCZs 4 (NJ<sup>2</sup>) and 5 (NJ<sup>3</sup>) showed only one HW event, while two other urban sites, WX (LCZ 2<sub>4</sub>) and YC (LCZ 2<sub>E</sub>), experienced five HW events with total HW durations of 20 to 23 days; their rural counterparts had no HW events during the same period. Based on the results of UHI intensity shown in Fig. 8, we found that the LCZ sites with weak UHIs experienced less frequent and shorter duration HW events, as seen when comparing the UHI and HW of LCZs 4 (NJ<sup>2</sup>) and 5 (NJ<sup>3</sup>) with those of other urban LCZ sites. However, based on Fig. 8 and Fig. 11, the frequencies and durations of HW events were not strictly proportional to the UHI intensities. The urban-rural differences in CW showed the opposite trend to that of HW. At least one CW was recorded at seven of the rural sites, while only one urban site (QD) experienced a CW. These results indicated that urban sites tended to experience less frequent and shorter duration CW events relative to rural sites. Overall, the urban LCZ sites had an intensifying effect on HW, but a mitigating effect on CW. This may be because urban LCZ sites were typically warmer than their rural surroundings for most of the year.

We selected the results from SQ to explore urban-rural differences in HW and CW events in more detail. Fig. 12a shows three HW events that occurred at the SQ urban site during the period from June to early September. As introduced in Section 2.6.1, a HW event is defined as having at least three consecutive days with both daily  $T_{\max}$  and  $T_{\min}$  above the Q90 ( $T_{\max}$ ) thresholds. For the rural site, there were more than three consecutive days with daily  $T_{\max}$  above the Q90 ( $T_{\max}$ ) thresholds, but the corresponding daily  $T_{\min}$  were often lower than the Q90 ( $T_{\min}$ ) thresholds. Therefore, according to the definition of HW, no HW events occurred at the rural site. The urban LCZ site

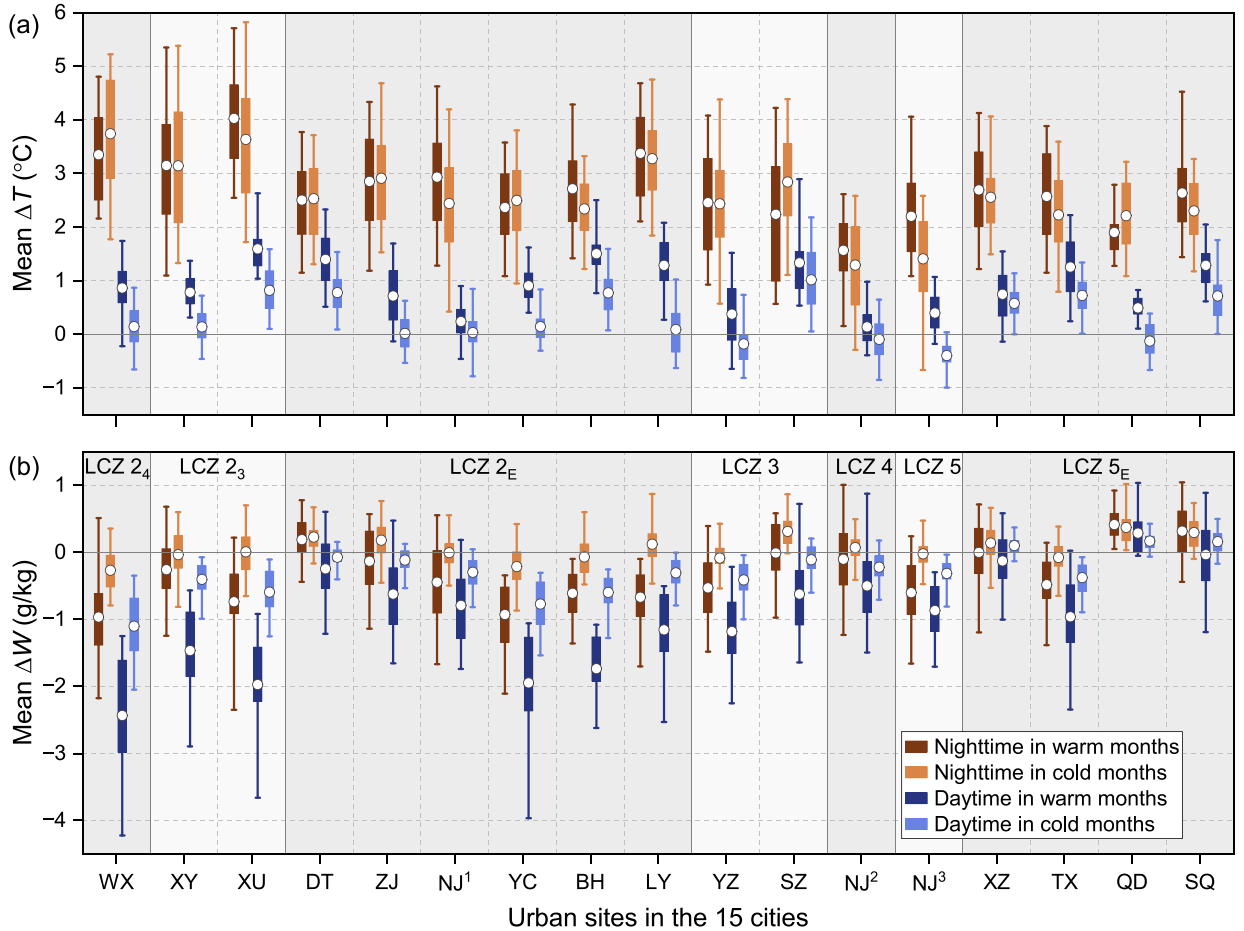


**Fig. 10.** Diurnal and seasonal changes in the mean  $\Delta T$  and  $\Delta W$  for ‘ideal’ days. Warm (cold) months are from April to September (October to March). The definitions of nighttime, daytime, LCZs, background grey shades, and boxplots are the same as Fig. 8.

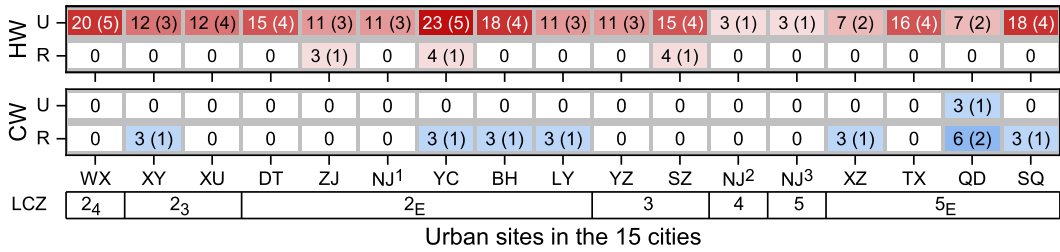


**Fig. 11.** Cumulative days (outside parentheses) and number of occurrences (inside parentheses) of heat wave (HW) and cold wave (CW) events for the 17 urban sites (U) and their rural counterparts (R) over the 1-year study period. The more HW/CW days, the deeper the fill colors.

generally exhibited higher daily  $T_{\max}$  and  $T_{\min}$  values than the rural site due to the UHI effect, resulting in three HW events during the study period. Similar phenomena were revealed for different LCZs in three cities of Belgium (Verdonck et al., 2018). As shown in Fig. 12b, in January, the rural site had three consecutive days where both daily  $T_{\max}$  and  $T_{\min}$  were below the Q10 thresholds. Therefore, it was determined that there was a CW event at the rural site. In contrast, the higher daily  $T_{\max}$  and  $T_{\min}$  at the urban site due to the UHI effect resulted in no CW events occurring. In short, both daily  $T_{\max}$  and  $T_{\min}$  values at urban built-up areas were typically elevated relative to their rural surroundings, which affected the frequencies and durations of HW and CW events. The significant urban-rural difference in HW and CW events implied that it is important to take local-scale variability in air temperatures into account during the assessment of HW and CW risks.

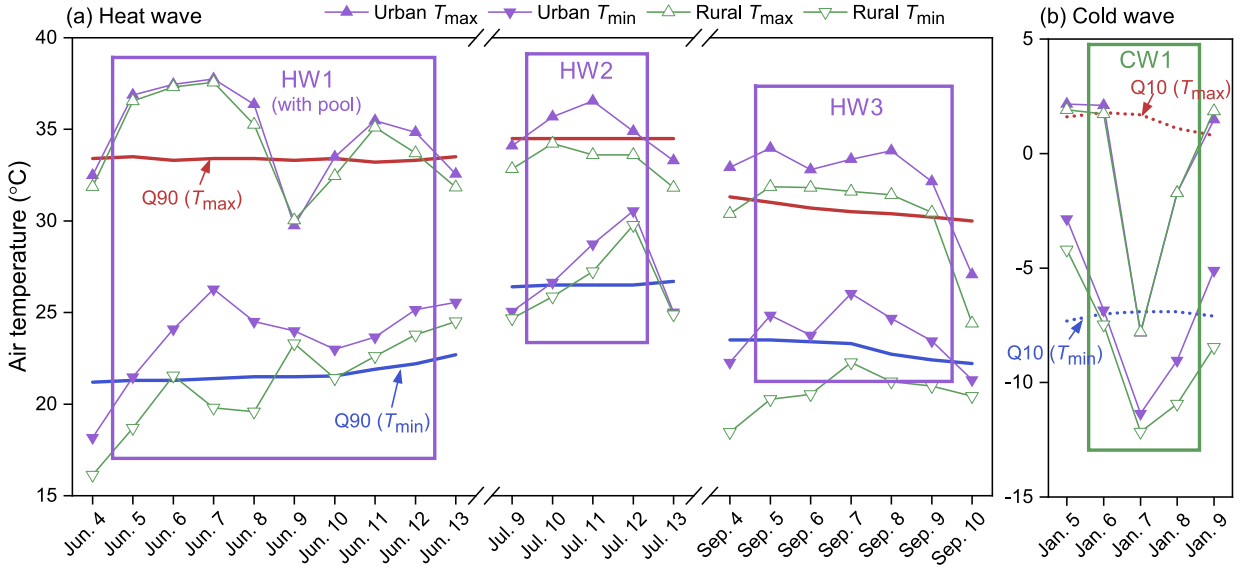


**Fig. 12.** Differences in heat and cold wave events between the urban and rural sites using SQ city as an example.  $T_{\max}$  and  $T_{\min}$  denote the daily maximum and minimum air temperatures, respectively. Q90 and Q10 denote the 90th and 10th percentiles of the historical observations from the 30-year baseline period. See Section 2.6.1 for detailed descriptions.

### 3.6.2. CDH and HDH

Fig. 13 shows the CDH and HDH for the urban and rural sites. For all sites, the values of HDH were much greater than those of CDH. This was related to the regional climate features of Jiangsu Province where the number of hours with temperatures below  $18^{\circ}\text{C}$  is much greater than the number of hours with temperatures above  $26^{\circ}\text{C}$ . In comparison with the rural reference sites, the urban sites

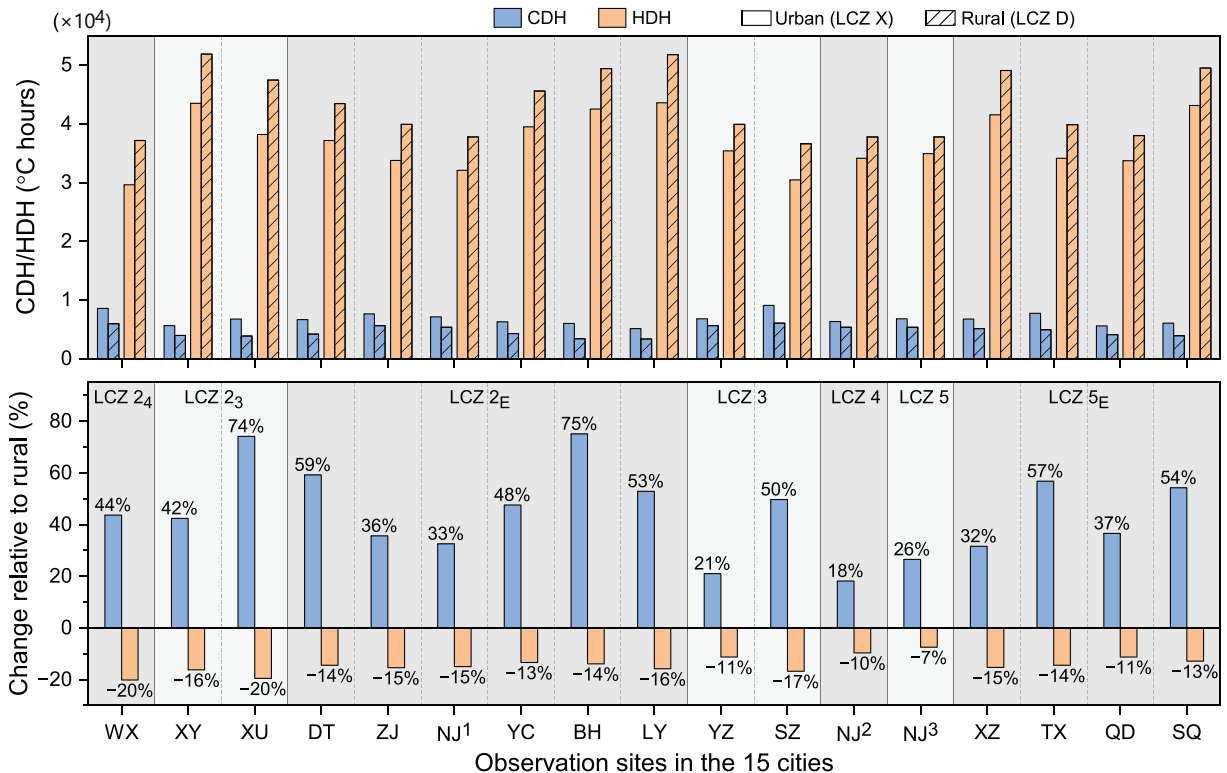


**Fig. 13.** Cooling degree hours (CDH) and heating degree hours (HDH) of the urban and rural sites (top) and percentage changes relative to their rural counterparts (bottom).

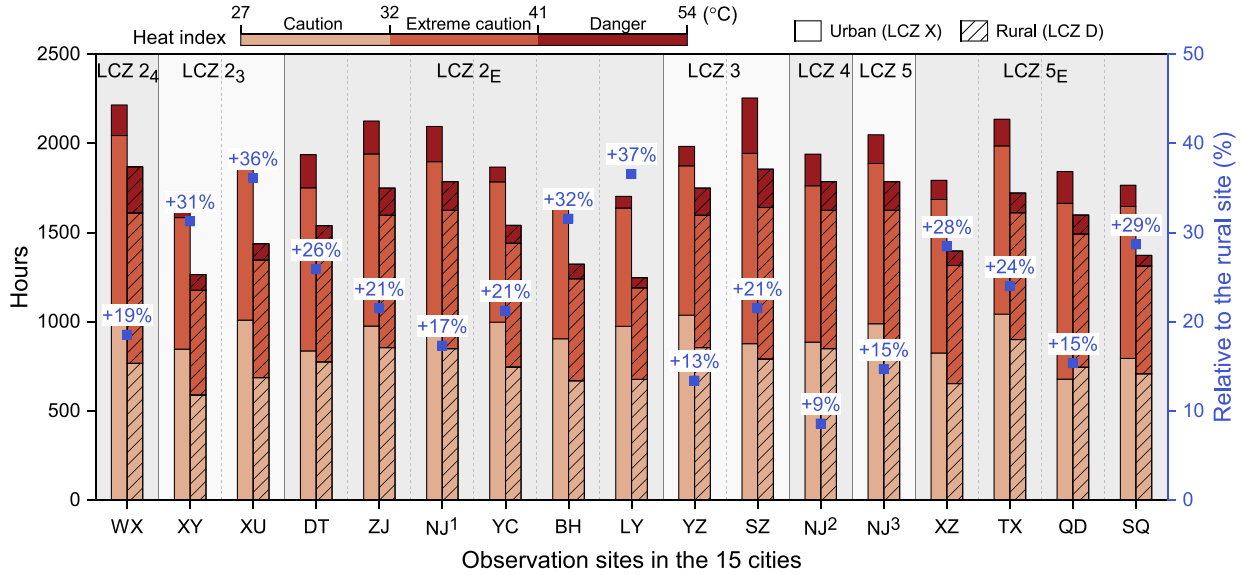


Fig. 14. Cumulative hours of Heat Index temperatures above the caution level at the 17 urban sites and their rural counterparts.

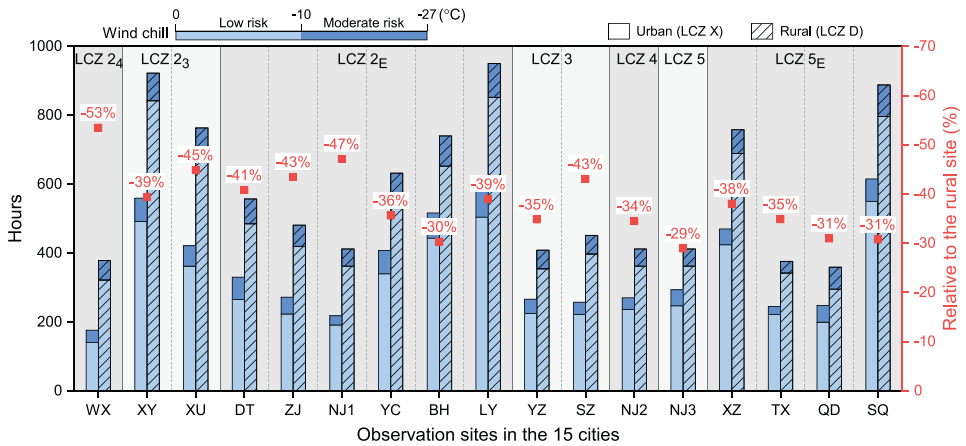


Fig. 15. Cumulative hours of Wind Chill temperatures exceeding the low-risk level at the 17 urban sites and their rural counterparts.

showed reductions in HDH by 7–20% and increases in CDH by 18–75%. Such differences in HDH and CDH could be because all urban sites featured UHI phenomena throughout the study period. In general, the sites with weaker UHIs, such as LCZs 4 and 5 (refer to Fig. 8), showed smaller differences in CDH and HDH relative to the rural sites. Our results demonstrated that significant increases in CDH and reductions in HDH are phenomena that commonly occur in variety of cities. These findings have important implications regarding the impacts of local-scale urban climates on building cooling and heating energy demands, which has attracted great attention in recent years (Li et al., 2019; Yang et al., 2020c).

### 3.6.3. HI and WC

Fig. 14 shows the cumulative hours of HI temperatures that exceeded the caution level for the urban and rural sites. As introduced in Section 2.6.3, HI is a measure that combines the effects of  $T$  and  $RH$ , and it increases with increasing  $T$  and  $RH$ . In comparison with the rural sites, the urban sites featured higher  $T$ , but lower  $RH$ . Therefore, at urban sites, the lower  $RH$  may offset the increases in HI due to increases in  $T$  by some extent. However, all urban sites experienced more hours (from 9% to 37% more) with HI temperatures above the caution level than their rural counterparts (Fig. 14). The modelled variability of human thermal stress in LCZs of Brno, Czech Republic (Geletić et al., 2018), and LCZs of Athens, Greece (Giannaros et al., 2023), showed similar trends. We found no clear pattern in the increases in the numbers of hours (i.e., HI above the caution level) for sites classified as the same LCZ type. Fig. 15 shows the cumulative hours of WC temperatures exceeding the low-risk level for the urban and rural sites. The results showed that there were no WC temperatures that exceeded the moderate risk level ( $<-27^{\circ}\text{C}$ ). For all urban sites, the numbers of hours when WC temperatures within the low to moderate risks levels were remarkably lower than their rural counterparts, with differences ranging from -29% to

–53%. This can be explained by the elevated air temperatures at urban sites due to the UHI effect. This results indicated that urban sites have significantly lower risk of low WC temperatures. Similar to the HI temperature results, no clear pattern in the lower numbers of hours of low WC temperatures was found for sites in the same LCZ classification. Our results clearly demonstrate the need to consider the effects of urban local climate on human thermal stress.

#### 4. Conclusions

This study has provided important insight into the general features of  $\Delta T$  and  $\Delta W$  (LCZ X – LCZ D), using 1-year of observations from 17 pairs of urban and rural sites for 15 cities in eastern China. In addition, we analyzed urban-rural differences in the frequencies and durations of heat and cold waves and the effects of local urban climates on building energy demands and human thermal stress.

The general features of  $\Delta T$  and  $\Delta W$ , as well as the key results of the three sets of assessment indices, are summarized below:

- (a) Diurnal cycles in  $\Delta T$  exhibited clear patterns under ‘ideal’ weather conditions: urban sites were significantly warmer than their rural counterparts during nighttime, but had lower and occasionally negative  $\Delta T$  during daytime. This was attributed to urban-rural differences in cooling and warming rates: for a few hours around sunset (after sunrise), urban sites had much slower cooling (warming) rates relative to the rural sites, which lead to the development (erosion) of UHIs. Daily maximum  $\Delta T$  mostly occurred during nighttime, and the 1st and 2nd halves of the nighttime period were not significantly different. The differences in  $\Delta T$  among different urban sites and various weather conditions were small and insignificant during daytime, and larger and more often significant at nighttime. The mean nocturnal  $\Delta T$  values for ‘ideal’ days showed distinctive differences among different LCZ classes. Furthermore, our results indicated that sites in different cities with similar surface structures and covers (i.e., classified as the same LCZ class) tended to exhibit approximately similar levels of UHI intensity. Additionally, no significant seasonality in the nocturnal  $\Delta T$  was found.
- (b) Both UMD and UME were commonly observed in the urban sites of different cities. For all urban sites, there was a non-negligible frequency of the occurrence of UME ( $\Delta W > 0.3 \text{ g/kg}$ ); and the frequencies of UME were higher during nighttime compared to daytime. For daily  $\Delta W$  extremes, extreme UMD events mostly occurred during daytime, while extreme UME events mostly occurred during nighttime. The differences in  $\Delta W$  among various weather conditions were insignificant. However, there were clear diurnal and seasonal patterns in the variability of  $\Delta W$ : larger urban-rural differences in  $W$  occurred during daytime and during warm months, as compared to nighttime and cold months, respectively. No clear patterns in inter-LCZ and intra-LCZ differences in  $\Delta W$  were found.
- (c) There were significant urban-rural differences in the three sets of assessment indices. Regarding HW and CW, both the frequencies and durations of HW events at urban sites were remarkably higher than those at the rural reference sites; however, urban sites tended to experience less frequent and shorter duration CW events. With respect to CDH and HDH, in comparison with the rural reference sites, urban sites had lower HDH by 7–20%, but higher CDH by 18–75%. With regard to HI and WC, for all urban sites, the number of hours with HI temperatures above the caution level were significantly higher than their rural counterparts by 9% to 37%. On the other hand, the number of hours when WC temperatures exhibited low or moderate risk were remarkably lower in urban sites than the rural counterparts, with differences ranging from –29% to –53%.

This study, however, had a few limitations. First, although the 15 studied cities are distributed in a wide geographical area, the diversity of climates is relatively limited, mainly representing a typical East Asia monsoon climate. Second, just one built-up LCZ site was selected for most cities and therefore intra-urban climate variability was not adequately investigated. Despite these limitations, the findings of this multi-city observational study have advanced our understanding of local-scale urban air temperature and humidity and their multi-dimensional influences, and thus will help in developing adaption and mitigation strategies to counter associated negative impacts in the future.

#### Funding

This work was supported by the National Natural Science Foundation of China [grant no. 41871189]; the Natural Science Foundation of Jiangsu Province, China [grant no. BK20201360]; the State Key Lab of Subtropical Building Science, South China University of Technology [grant no. 2021ZB01]; and the Startup Foundation for Introducing Talent of NUIST.

#### CRediT authorship contribution statement

**Xiaoshan Yang:** Conceptualization, Methodology, Investigation, Writing – original draft, Visualization, Supervision, Project administration, Funding acquisition. **Shasha Xu:** Investigation, Data curation. **Lilliana L.H. Peng:** Funding acquisition, Writing – review & editing. **Yuan Chen:** Investigation. **Lingye Yao:** Investigation.

#### Declaration of Competing Interest

The authors declare the following financial interests/personal relationships which may be considered as potential competing interests.

Lilliana L.H. Peng reports financial support was provided by National Natural Science Foundation of China. Xiaoshan Yang reports

financial support was provided by Natural Science Foundation of Jiangsu Province, China. Xiaoshan Yang reports financial support was provided by the State Key Lab of Subtropical Building Science, South China University of Technology. Xiaoshan Yang reports financial support was provided by the Startup Foundation for Introducing Talent of NUIST.

## Data availability

The authors do not have permission to share data.

## Acknowledgements

The authors would like to acknowledge the China Meteorological Data Service Centre for the data used in this study and Mr. Ackley Lane at University of Oregon for the English language review.

## Appendix A. Supplementary data

Supplementary data to this article can be found online at <https://doi.org/10.1016/j.ulclim.2023.101652>.

## References

- Anderson, G.B., Bell, M.L., Peng, R.D., 2013. Methods to calculate the heat index as an exposure metric in environmental health research. *Environ. Health Perspect.* 121 (10), 1111–1119. <https://doi.org/10.1289/ehp.1206273>.
- Anjos, M., Targino, A.C., Kreci, P., Oukawa, G.Y., Braga, R.F., 2020. Analysis of the urban heat island under different synoptic patterns using local climate zones. *Build. Environ.* 185, 107268 <https://doi.org/10.1016/j.buildenv.2020.107268>.
- Beck, C., Straub, A., Breitner, S., Cyrys, J., Philipp, A., Rathmann, J., Schneider, A., Wolf, K., Jacobbeit, J., 2018. Air temperature characteristics of local climate zones in the Augsburg urban area (Bavaria, southern Germany) under varying synoptic conditions. *Urban Clim.* 25, 152–166. <https://doi.org/10.1016/j.ulclim.2018.04.007>.
- Bróde, P., Fiala, D., Blažejczyk, K., Holmér, I., Jendritzky, G., Kampmann, B., et al., 2012. Deriving the operational procedure for the universal thermal climate index (UTCI). *Int. J. Biometeorol.* 56 (3), 481–494. <https://doi.org/10.1007/s00484-011-0454-1>.
- Chen, X., Yang, J., Ren, C., Jeong, S., Shi, Y., 2021. Standardizing thermal contrast among local climate zones at a continental scale: implications for cool neighborhoods. *Build. Environ.* 197, 107878 <https://doi.org/10.1016/j.buildenv.2021.107878>.
- China Meteorological Data Service Centre (CMDC). Retrieved from. <http://data.cma.cn/en>. Last assess: 10 December 2022.
- Coccato, S., Kämpf, J., Scartezzini, J., Pearlmutter, D., 2016. Outdoor human comfort and thermal stress: a comprehensive review on models and standards. *Urban Clim.* 18, 33–57. <https://doi.org/10.1016/j.ulclim.2016.08.004>.
- De Luminæe, 2022. DL-Light Extension for SketchUp (Version 14.0.11). retrieved from. <https://deluminaelab.com/dl-light/en/>. Last assess: 8 February 2022.
- Dunjić, J., Milošević, D., Kojić, M., Savić, S., Lužanin, Ž., Šćerov, I., Arsenović, D., 2021. Air humidity characteristics in “Local Climate Zones” of Novi Sad (Serbia) based on long-term data. *ISPRS Int. J. Geo Inf.* 10 (12), 810. <https://doi.org/10.3390/ijgi10120810>.
- Emery, J., Pohl, B., Crétat, J., Richard, Y., Pergaud, J., Rega, M., Zito, S., Dudek, J., Vairet, T., Joly, D., Thévenin, T., 2021. How local climate zones influence urban air temperature: measurements by bicycle in Dijon, France. *Urban Clim.* 40, 101017 <https://doi.org/10.1016/j.ulclim.2021.101017>.
- Estrada, F., Botzen, W.J.W., Tol, R.S.J., 2017. A global economic assessment of city policies to reduce climate change impacts. *Nat. Clim. Chang.* 7 (6), 403–406. <https://doi.org/10.1038/nclimate3301>.
- European Drought Observatory, 2021. EDO Heat and Cold Wave Index (version 1.0.0). <http://data.europa.eu/89h/c9e06815-0c52-4ff5-b596-89ec169996eb>. Last access: 10 April 2022.
- Fenner, D., Meier, F., Bechtel, B., Otto, M., Scherer, D., 2017. Intra and inter ‘local climate zone’ variability of air temperature as observed by crowdsourced citizen weather stations in Berlin, Germany. *Meteorol. Z.* 26 (5), 525–547. <https://doi.org/10.1127/metz/2017/0861>.
- Geletič, J., Lehnhert, M., Savić, S., Milošević, D., 2018. Modelled spatiotemporal variability of outdoor thermal comfort in local climate zones of the city of Brno, Czech Republic. *Sci. Total Environ.* 624, 385–395. <https://doi.org/10.1016/j.scitotenv.2017.12.076>.
- Giannaros, C., Agathangelidis, I., Papavasileiou, G., Galanaki, E., Kotroni, V., Lagouvardos, K., Giannaros, T.M., Cartalis, C., Matzarakis, A., 2023. The extreme heat wave of July–August 2021 in the Athens urban area (Greece): atmospheric and human-biometeorological analysis exploiting ultra-high resolution numerical modeling and the local climate zone framework. *Sci. Total Environ.* 857, 159300 <https://doi.org/10.1016/j.scitotenv.2022.159300>.
- Grimm, N.B., Faeth, S.H., Golubiewski, N.E., Redman, C.L., Wu, J., Bai, X., Briggs, J.M., 2008. Global change and the ecology of cities. *Science* 319, 756–760. <https://doi.org/10.1126/science.1150195>.
- Ho, J.Y., Shi, Y., Lau, K.K.L., Ng, E.Y.Y., Ren, C., Goggins, W.B., 2023. Urban heat island effect-related mortality under extreme heat and non-extreme heat scenarios: a 2010–2019 case study in Hong Kong. *Sci. Total Environ.* 858, 159791 <https://doi.org/10.1016/j.scitotenv.2022.159791>.
- Hoppe, P., 1999. The physiological equivalent temperature - a universal index for the biometeorological assessment of the thermal environment. *Int. J. Biometeorol.* 43 (2), 71–75. <https://doi.org/10.1007/s004840050118>.
- Jiang, S., Zhan, W., Dong, P., Wang, C., Li, J., Miao, S., Jiang, L., Du, H., Wang, C., 2022. Surface air temperature differences of intra- and inter-local climate zones across diverse timescales and climates. *Build. Environ.* 222, 109396 <https://doi.org/10.1016/j.buildenv.2022.109396>.
- Jiangsu Phoenix Science Press, 2014. Design Standard of Thermo-Environment and Energy Conservation for Residential Buildings in Jiangsu Province (DGJ32/J 71-2014) (in Chinese).
- Kabano, P., Lindley, S., Harris, A., 2021. Evidence of urban heat island impacts on the vegetation growing season length in a tropical city. *Landsc. Urban Plan.* 206, 103989 <https://doi.org/10.1016/j.landurbplan.2020.103989>.
- Kotharkar, R., Bagade, A., 2018. Evaluating urban heat island in the critical local climate zones of an Indian city. *Landsc. Urban Plan.* 169, 92–104. <https://doi.org/10.1016/j.landurbplan.2017.08.009>.
- Laaidi, K., Zeghnoun, A., Dousset, B., Bretin, P., Vandentorren, S., Giraudet, E., Beaudeau, P., 2012. The impact of heat islands on mortality in Paris during the August 2003 heat wave. *Environ. Health Perspect.* 120 (2), 254–259. <https://doi.org/10.1289/ehp.1103532>.
- Lavaysse, C., Cammalleri, C., Dosio, A., van der Schrier, G., Toreti, A., Vogt, J., 2018. Towards a monitoring system of temperature extremes in Europe. *Nat. Hazards Earth Syst. Sci.* 18 (1), 91–104. <https://doi.org/10.5194/nhess-18-91-2018>.
- Leconte, F., Bouyer, J., Claverie, R., Pétrissans, M., 2015. Using local climate zone scheme for UHI assessment: evaluation of the method using mobile measurements. *Build. Environ.* 83, 39–49. <https://doi.org/10.1016/j.buildenv.2014.05.005>.
- Leconte, F., Bouyer, J., Claverie, R., 2020. Nocturnal cooling in local climate zone: statistical approach using mobile measurements. *Urban Clim.* 33, 100629 <https://doi.org/10.1016/j.ulclim.2020.100629>.

- Lehnert, M., Geletić, J., Husák, J., Vysoudil, M., 2015. Urban field classification by “local climate zones” in a medium-sized central European city: the case of Olomouc (Czech Republic). *Theor. Appl. Climatol.* 122 (3–4), 531–541. <https://doi.org/10.1007/s00704-014-1309-6>.
- Li, X., Zhou, Y., Yu, S., Jia, G., Li, H., Li, W., 2019. Urban heat island impacts on building energy consumption: a review of approaches and findings. *Energy* 174, 407–419. <https://doi.org/10.1016/j.energy.2019.02.183>.
- Liu, H., Huang, B., Yang, C., 2020. Assessing the coordination between economic growth and urban climate change in China from 2000 to 2015. *Sci. Total Environ.* 732, 139283 <https://doi.org/10.1016/j.scitotenv.2020.139283>.
- Liu, H., Tong, M., Guo, F., Nie, Q., Li, J., Li, P., Zhu, T., Xue, T., 2022. Deaths attributable to anomalous temperature: a generalizable metric for the health impact of global warming. *Environ. Int.* 169, 107520 <https://doi.org/10.1016/j.envint.2022.107520>.
- McGregor, G.R., Bessemoulin, P., Ebi, K., Menne, B., 2015. Heatwaves and Health: Guidance on Warning-System Development. World Meteorological Organization and World Health Organization, p. xi. Retrieved from. <https://www.who.int/docs/default-source/climate-change/heat-waves-and-health—guidance-on-warning-system-development.pdf>. Last access: 5 May 2022.
- Milošević, D., Savić, S., Kresojá, M., Lužanin, Ž., Šećerov, I., Arsenović, D., Dunjić, J., Matzarakis, A., 2022. Analysis of air temperature dynamics in the “local climate zones” of Novi Sad (Serbia) based on long-term database from an urban meteorological network. *Int. J. Biometeorol.* 66 (2), 371–384. <https://doi.org/10.1007/s00484-020-02058-w>.
- National Oceanic and Atmospheric Administration, 2022. National Weather Service. <https://www.weather.gov/safety/>. Last assess: 15 October 2022.
- Núñez-Péiró, M., Sánchez-Guevara Sánchez, C., Neila González, F.J., 2021. Hourly evolution of intra-urban temperature variability across the local climate zones. The case of Madrid. *Urban Clim.* 39, 100921 <https://doi.org/10.1016/j.ul clim.2021.100921>.
- Oke, T.R., 2006. Initial Guidance to Obtain Representative Meteorological Observations at Urban Sites. World Meteorological Organization, Geneva, Switzerland. Retrieved from. [https://library.wmo.int/doc\\_num.php?explnum\\_id=9286](https://library.wmo.int/doc_num.php?explnum_id=9286). Last access: 12 May 2022.
- Oke, T.R., Mills, G., Christen, A., Voogt, J.A., 2017. *Urban climates*. Cambridge University Press.
- Papakostas, K., Kyriakis, N., 2005. Heating and cooling degree-hours for Athens and Thessaloniki, Greece. *Renew. Energy* 30 (12), 1873–1880. <https://doi.org/10.1016/j.renene.2004.12.002>.
- Qi, F., Wang, Y., 2014. A new calculation method for shape coefficient of residential building using Google earth. *Energ. Build.* 76, 72–80. <https://doi.org/10.1016/j.enbuild.2014.02.058>.
- Richard, Y., Emery, J., Dudek, J., Pergaud, J., Chateau-Smith, C., Zito, S., Rega, M., Vairet, T., Castel, T., Thévenin, T., Pohl, B., 2018. How relevant are local climate zones and urban climate zones for urban climate research? Dijon (France) as a case study. *Urban Clim.* 26, 258–274. <https://doi.org/10.1016/j.ul clim.2018.10.002>.
- Santamouris, M., 2015. Analyzing the heat island magnitude and characteristics in one hundred Asian and Australian cities and regions. *Sci. Total Environ.* 512–513, 582–598. <https://doi.org/10.1016/j.scitotenv.2015.01.060>.
- Shi, Y., Zhang, Y., 2022. Urban morphological indicators of urban heat and moisture islands under various sky conditions in a humid subtropical region. *Build. Environ.* 214, 108906 <https://doi.org/10.1016/j.buildenv.2022.108906>.
- Shi, Y., Lau, K.K., Ren, C., Ng, E., 2018. Evaluating the local climate zone classification in high-density heterogeneous urban environment using mobile measurement. *Urban Clim.* 25, 167–186. <https://doi.org/10.1016/j.ul clim.2018.07.001>.
- Skarbit, N., Stewart, I.D., Unger, J., Gál, T., 2017. Employing an urban meteorological network to monitor air temperature conditions in the ‘local climate zones’ of Szeged, Hungary. *Int. J. Climatol.* 37, 582–596. <https://doi.org/10.1002/joc.5023>.
- Stewart, I.D., 2011. A systematic review and scientific critique of methodology in modern urban heat island literature. *Int. J. Climatol.* 31 (2), 200–217. <https://doi.org/10.1002/joc.2141>.
- Stewart, I.D., Oke, T.R., 2012. Local climate zones for urban temperature studies. *Bull. Am. Meteorol. Soc.* 93 (12), 1879–1900. <https://doi.org/10.1175/BAMS-D-11-00019.1>.
- Stewart, I.D., Oke, T.R., Krayenhoff, E.S., 2014. Evaluation of the ‘local climate zone’ scheme using temperature observations and model simulations. *Int. J. Climatol.* 34 (4), 1062–1080. <https://doi.org/10.1002/joc.3746>.
- The U.S. Department of Energy, 2022. EnergyPlus (Version 22.1.0). Retrieved from. <https://energyplus.net/>. Last assess: 20 April 2022.
- Top, S., Milošević, D., Caluwaerts, S., Hamdi, R., Savić, S., 2020. Intra-urban differences of outdoor thermal comfort in Ghent on seasonal level and during record-breaking 2019 heat wave. *Build. Environ.* 185, 107103 <https://doi.org/10.1016/j.buildenv.2020.107103>.
- Unger, J., Skarbit, N., Gál, T., 2018a. Absolute moisture content in mid-latitude urban canopy layer, Part 1: a literature review. *Acta Climatol.* 51–52, 37–45. <https://doi.org/10.14232/acta.clim.2018.52.2>.
- Unger, J., Skarbit, N., Gál, T., 2018b. Evaluation of outdoor human thermal sensation of local climate zones based on long-term database. *Int. J. Biometeorol.* 62 (2), 183–193. <https://doi.org/10.1007/s00484-017-1440-z>.
- Verdonck, M., Demuzere, M., Hooyberghs, H., Beck, C., Cyrys, J., Schneider, A., Dewulf, R., Van Coillie, F., 2018. The potential of local climate zones maps as a heat stress assessment tool, supported by simulated air temperature data. *Landsc. Urban Plan.* 178, 183–197. <https://doi.org/10.1016/j.landurbplan.2018.06.004>.
- Yang, X., Yao, L., Jin, T., Peng, L.L.H., Jiang, Z., Hu, Z., Ye, Y., 2018. Assessing the thermal behavior of different local climate zones in the Nanjing metropolis, China. *Build. Environ.* 137, 171–184. <https://doi.org/10.1016/j.buildenv.2018.04.009>.
- Yang, X., Chen, Y., Peng, L.L.H., Wang, Q., 2020a. Quantitative methods for identifying meteorological conditions conducive to the development of urban heat islands. *Build. Environ.* 178, 106953 <https://doi.org/10.1016/j.buildenv.2020.106953>.
- Yang, X., Peng, L.L.H., Chen, Y., Yao, L., Wang, Q., 2020b. Air humidity characteristics of local climate zones: a three-year observational study in Nanjing. *Build. Environ.* 171, 106661 <https://doi.org/10.1016/j.buildenv.2020.106661>.
- Yang, X., Peng, L.L.H., Jiang, Z., Chen, Y., Yao, L., He, Y., Xu, T., 2020c. Impact of urban heat island on energy demand in buildings: local climate zones in Nanjing. *Appl. Energy* 260, 114279. <https://doi.org/10.1016/j.apenergy.2019.114279>.
- Zhao, C., Weng, Q., Wang, Y., Hu, Z., Wu, C., 2022a. Use of local climate zones to assess the spatiotemporal variations of urban vegetation phenology in Austin, Texas, USA. *GISci. Remot. Sens.* 59 (1), 393–409. <https://doi.org/10.1080/15481603.2022.2033485>.
- Zhao, M., Cheng, C., Zhou, Y., Li, X., Shen, S., Song, C., 2022b. A global dataset of annual urban extents (1992–2020) from harmonized nighttime lights. *Earth Syst. Sci. Data* 14. <https://doi.org/10.5194/essd-14-517-2022>.